

#### FACULTY OF MEDICINE

DEPARTMENT OF ANATOMY, HISTOLOGY, CYTOLOGY AND BIOLOGY

# DESISLAVA MARINOVA MARINOVA

Study of the expression of choline acetyltransferase mRNA alternative splicing isoforms in the mouse enteric nervous system

# **ABSTRACT**

#### from

a dissertation for granting of the educational and scientific degree DOCTOR

PhD program: Anatomy, histology and cytology

**Scientific supervisor:** 

Assoc. Prof. Stefan Trifonov, PhD

The dissertation comprises 126 standard pages and is structured into the following sections: Introduction, Literature Review, Aims, Objectives and Methodological Approaches, Results, Discussion of the Results, Conclusion, Findings, Contributions, and Future Directions.

The work is illustrated with 5 tables and 33 figures and includes two appendices. The bibliography comprises 270 references. The laboratory work and molecular analyses were conducted at the Department of Anatomy, Histology, Cytology, and Biology, Section of Anatomy, Histology, and Cytology, Faculty of Medicine, Medical University of Pleven, and at the University Laboratory for Scientific Research, Medical University of Pleven.

In connection with the dissertation, three full-text publications and four scientific presentations at national forums have been produced.

The dissertation has been approved and referred for public defense by the Department Council at the Anatomy, Histology, Cytology and Biology Department of the Faculty of Medicine of the Medical University of Pleven held on the 23 September 2025.

The public defense of the dissertation will take place on the 01.12.2025 in Ambroaz Pare Hall of the Medical University of Pleven according to the rules and regulations on obtaining scientific degrees and occupation of academic positions of the Medical University of Pleven and on the grounds of Order No 4059/28.10.2025 of the Rector of the University in front of the following scientific jury:

### **Chairperson:**

Prof. Stefan Sivkov, PhD, MD

#### **Members:**

Prof. Ivan Maslarski, PhD, MD

Prof. Nikolay Dimitrov, PhD, MD

Prof. Dimitar Sivrey, PhD, MD

Prof. Galya Stavreva, PhD, MD

#### Official examiners:

Prof. Stefan Sivkov, PhD, MD

Prof. Dimitar Sivrey, PhD, MD

The materials related to the defence have been published on the website of the Medical University of Pleven: http://www.mu-pleven.bg/index.php/bg/.

# **Abbreviations and Terminology**

ENS – Enteric nervous system

Ach - Acetylcholine

ChAT – Choline acetyltransferase

GIT – Gastrointestinal tract

CNS – Central nervous system

mRNA – Messenger RNA

cChAT – Common type of ChAT

pChAT – Peripheral type of ChAT

CHT – High-affinity choline transporter

VAChT – Vesicular acetylcholine transporter

NO – Nitric oxide

VIP – Vasoactive intestinal peptide

ATP – Adenosine-5′-triphosphate

CO – Carbon monoxide

ICC – Interstitial cells of Cajal

EGCs – Enteric glial cells

5-HT – 5-hydroxytryptamine (serotonin)

IPANs – Intrinsic primary afferent neurons

PARs – Protease-activated receptors

SOM – Somatostatin

TK – Tyrosine kinase

NPY – Neuropeptide Y

CGRP – Calcitonin Gene-Related Peptide

NADH – Nicotinamide Adenine Dinucleotide

NADH-d – Reduced form of NADH

PCR – Polymerase Chain Reaction

RT-PCR – Reverse Transcription Polymerase Chain Reaction

PBS – Phosphate-Buffered Saline

Open Reading Frame – Nucleotide sequences located between the initiating and terminating codon

Primer – Single-stranded synthetic oligonucleotide complementary to a specific nucleotide region of the template DNA

Tm – Melting temperature – the temperature at which half of the DNA fragment is double-stranded and the other half is single-stranded; Tm depends on fragment length and GC content

GAPDH – Glyceraldehyde-3-phosphate dehydrogenase

# **Table of content**

I. Introduction	6
II. Purpose, tasks, and methodological approaches	9
1. Purpose	9
2. Tasks	9
3. Materials and Methods	9
3.1. Light microscopy methods for the preparation of permanent histological stained with hematoxylin-eosin	
3.2. Analysis and primer design for the splicing variants of the enzyme cholin acetyltransferase	e
3.3. De novo design of double-stranded gBlock gene fragments and pGEM-Ni plasmid used in PCR reactions to test the specificity of isoform-specific prime	
3.4. Conventional polymerase chain reaction	15
3.5. Construction of standard curves to determine amplification efficiency of primer pair	
3.6. Isolation of RNA from experimental animals	
3.7. Synthesis of complementary DNA (cDNA)	
3.8. Quantitative PCR using specific primer pairs and cDNA from the stomad duodenum, jejunum, ileum, and colon of C57BL/6NCrl mice	
3.9. Statistical analysis	19
III. Results	20
1. Histological organization of the wall of the digestive tract of C57Bl/6NCrl	mice20
2. Testing the specificity of <i>de novo</i> synthesized primer pairs and DNA temp conventional real-time PCR	
3. Relative quantitative analysis of the expression of ChAT mRNA isoforms	26
3.1. Generation of standard curves	26
3.2. Determination of the amplification efficiency of each primer pair	30
3.3. Expression of ChAT isoforms across mouse gastrointestinal tract via real PCR	
3.4. Relative quantitative PCR analysis of ChAT isoforms expression across of regions of the gastrointestinal tract in C57Bl/6NCrl mice	
IV. Discussion	44
1. Histological features of the digestive tract wall in C57Bl/6NCrl mice	44

2. Functional organization of the ENS	
3. Genetic analysis of ChAT: molecular strategies for ident	ifying and visualizing
ChAT isoforms in the mice	48
V. Conclusion	56
VI. Deductions	57
VII. Contributions	58
VIII. Future directions and perspectives	59
IX. Publications, participation in scientific forums and scientif	fic project related to the
dissertation	60
Appendix 1	61
Appendix 2	65

### I. Introduction

The enteric nervous system (ENS) is a distinct component of the autonomic division of the nervous system, comprising neuronal circuits responsible for controlling motor functions, local blood flow, mucosal transport, and secretion. In addition to its motor and secretory functions, the cellular components of the ENS communicate closely with the gut microbiome. Contemporary studies highlight the critical role of the gut-microbiome-brain axis in maintaining gut health, immune function, and the neuropsychological well-being of the entire organism. To accomplish its diverse functions, this "third division" of the autonomic nervous system consists of a wide variety of neurons forming reflex circuits, some of which are confined to local networks.

Within the ENS, four distinct plexuses are described, which differ in their localization, the presence or absence of well-defined ganglia, and their target effector structures. Beneath the serosal layer of the gastrointestinal tract (GIT) lies the subserosal plexus, first described by Auerbach, consisting of a fine network of nerve fibers located within the underlying subserosal connective tissue. The myenteric plexus (plexus myentericus, Auerbach) represents the primary and most prominent plexus, situated between the inner (circular) and outer (longitudinal) muscle layers. Among the fibers of the circular muscle layer lies a secondary plexus, while a tertiary plexus is positioned among the fibers of the longitudinal muscle layer. Myenteric ganglia in this plexus vary in size, shape, and orientation between animal species. The submucosal plexus (plexus submucosus, Meissner) lies in the connective tissue layer between the mucosa and the muscular coat of the GIT. First described in the mid-19th century by Meissner and Billroth, it is organized into two sublayers – the outer (Shabadasch) and inner (Meissner) plexuses. Ganglia in the submucosal plexus are significantly smaller in size compared to those of the myenteric plexus.

Enteric neurons within the ENS exert their functions through a rich repertoire of neurotransmitters. The principal approaches to neuron classification include their external morphology, functional properties, electrophysiological features, and neurochemical profile. Methods employed to determine the neurochemical identity of enteric neurons include histochemical, immunohistochemical, and modern genetic techniques, enabling the study of enzymes responsible for neurotransmitter synthesis within the ENS. Knowledge of the chemical coding of neurons allows the identification of distinct classes of enteric neurons based on their unique combinations of chemical markers. The neurochemical code of enteric neurons is closely related to their functional specialization, localization, and the types of connections they establish within the ENS.

Cholinergic neurotransmission in the ENS is well established and plays a key role in mediating motor, secretory, intrinsic sensory, and vascular reflexes. Acetylcholine (ACh) is the principal neurotransmitter in excitatory motor neurons, along with tachykinins and calretinin. In ascending interneurons, tachykinins and ATP act as secondary neurotransmitters alongside ACh, whereas in descending interneurons the action of ACh is complemented by nitric oxide (NO), 5-hydroxytryptamine (5-HT), ATP, and somatostatin (SOM). In intrinsic primary afferent neurons (IPANs), ACh is the main neurotransmitter, with calcitonin gene-related peptide (CGRP) and tachykinins as co-transmitters.

ACh is synthesized in the cytoplasm of cholinergic neurons from choline and acetyl-CoA, in a reaction catalyzed by the enzyme choline acetyltransferase (ChAT). The rate-limiting step in ACh biosynthesis is the active transport of choline into nerve terminals via the Na<sup>+</sup>-dependent high-affinity choline transporter (CHT). Newly synthesized Ach is subsequently translocated into synaptic vesicles via the vesicular acetylcholine transporter (VAChT), a 12-transmembrane-domain protein that uses the electrochemical gradient generated by a proton ATPase to exchange two protons for one molecule of ACh.

Genetic studies have revealed a unique organization of the gene encoding ChAT. In mice, the ChAT gene is located on the long arm of chromosome 10 (10q11.23) and consists of 17 exons – 14 coding and 3 non-coding. There are three 5'-noncoding exons R, N, and M (Fig. 1A), followed by the 14 successive coding exons (Fig. 1B). The entire open reading frame of VAChT mRNA is located within the first intron of the ChAT gene locus, between R and N noncoding exons. Between the N exon and the first N-terminal coding ChAT exon is located the third M noncoding exon.

Seven differentially spliced mRNA isoforms (M, N1, N2, R1, R2, R3, and R4) have been identified in the mouse genome, compared to five variants in rats (R1, R2, N1, N2, and M). To date, seven splice isoforms have been described in primates and humans (R1/R2, N1/N2, H, S, and M). All these alternative splicing isoforms differ in their 5′-noncoding ends; therefore, all the transcripts encode the same protein with a molecular weight of 67 kDa in mice and rats, and 69 kDa in humans – referred to as the common type ChAT (cChAT). The functional role of these noncoding exons remains insufficiently understood, but they are believed to influence stability, translational efficiency, compartmentalization, and the three-dimensional structure of their respective mRNA isoforms. The presence of several different promoter regions raises the possibility that different types of ChAT mRNA may be expressed in various cholinergic neurons and non-neuronal cell types.

An alternative ChAT mRNA splice isoform in mice lacking the coding sequence corresponding to exons 5–8 has been described in peripheral neurons, nerve fibers, and non-neuronal structures. The translation product of this isoform has a molecular weight of 49 kDa. Because of the dominant expression in peripheral tissues, the novel variant has been termed ChAT of the peripheral type (pChAT), in contrast to the full-length one present in both the central and peripheral nervous systems, known as the common type (cChAT).

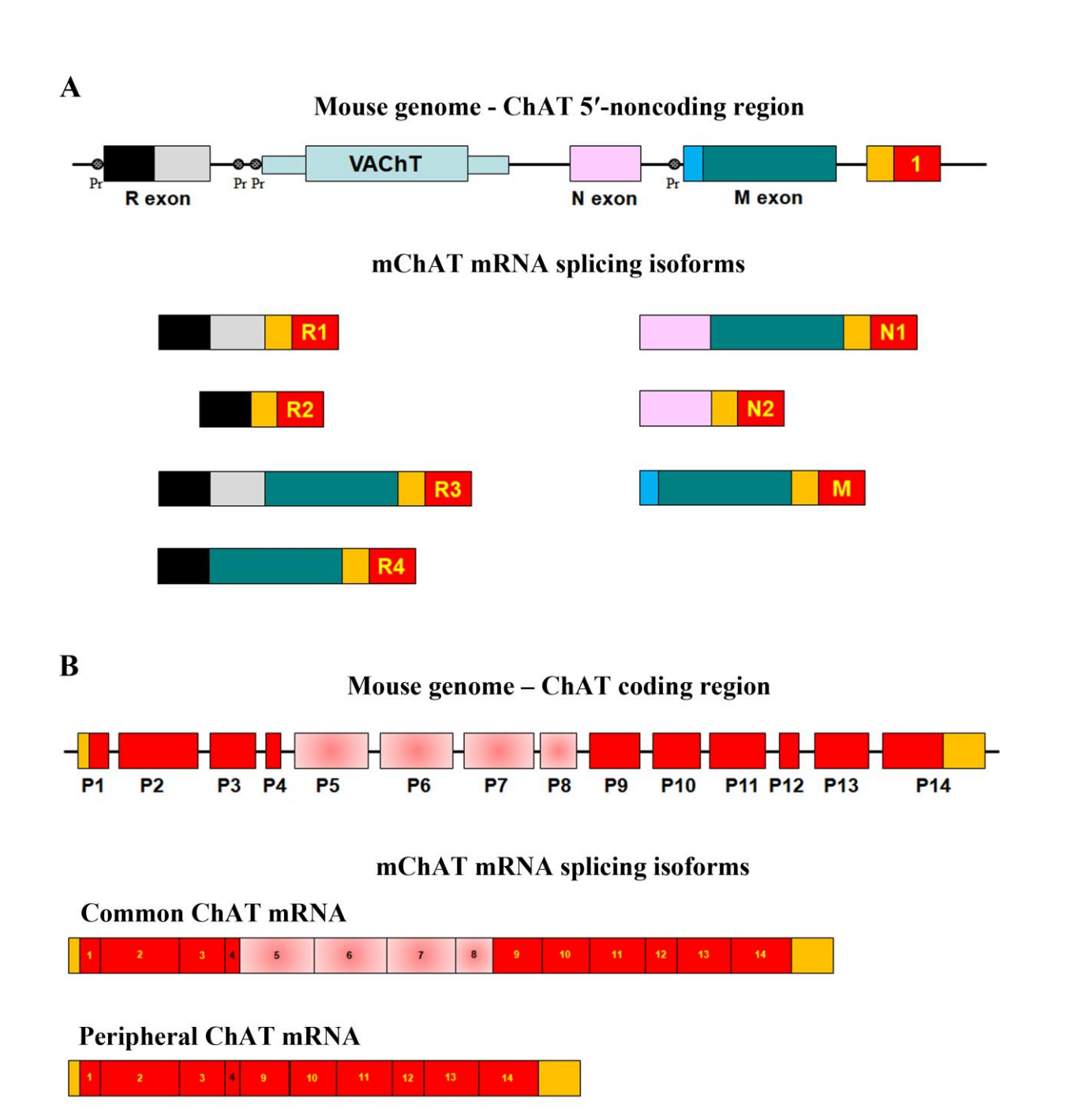


**Figure 1.** Schematic diagram showing the structure of cholinergic gene locus and the splicing pattern of multiple ChAT mRNA species. **A)** 5'-noncoding region and isoforms produced by alternative splicing of R, N and M noncoding exons. **B)** Coding region and the two alternatively spliced isoforms – cChAT and pChAT. Pr, promotor region; cChAT, common choline acetyltransferase; pChAT, peripheral choline acetyltransferase.

### II. Purpose, tasks, and methodological approaches

### 1. Purpose

- 1.1. Investigate the histological architecture of the gastrointestinal wall in C57Bl/6NCrl mice using the Swiss roll technique.
- 1.2. Examine the expression of mRNA splicing isoforms of the ChAT enzyme in the gastrointestinal tract of C57Bl/6NCrl mice.

### 2. Tasks

The scientific purpose of the dissertation is accomplished by completing the following tasks:

- 2.1. Collecting samples from different regions of the gastrointestinal tract of C57Bl/6NCrl mice for the preparation of permanent histological slides.
- 2.2. Analysis of the nucleotide sequences of alternatively splice isoform of mouse ChAT mRNA.
- 2.3. *In silico* design of specific primer pairs for PCR amplification splice isoform of mouse ChAT mRNA.
- 2.4. Test the specificity of the primer pairs using conventional PCR and gel electrophoresis. Optimize PCR reaction conditions.
- 2.5. Determine the amplification efficiency of each primer pair by analyzing standard curves.
- 2.6. Collect biological material and isolate total RNA from different regions of the mouse GIT (stomach, duodenum, jejunum, ileum and colon).
- 2.7. Perform reverse transcription to obtain copy DNA (cDNA).
- 2.8. Quantitative PCR using specific primer pairs for each ChAT splice isoform.

#### 3. Materials and Methods

To achieve the study aim and objectives, experimental mice of the C57Bl/6NCrl strain, aged between 9 and 11 weeks were used. The following methodological approaches were applied:

# 3.1. Light microscopy methods for the preparation of permanent histological slides stained with hematoxylin-eosin

The Swiss roll technique is a suitable method for the analysis of the murine GIT, which is characterized by a delicate wall structure. This approach facilitates the examination of long tissue segments along the GIT using cross-sections obtained from the rolled-up tissue samples. During the study, the animals were anesthetized intraperitoneally with a combination of Ketamine (100 mg/kg) and Xylazine (10 mg/kg). Two of the experimental animals underwent intracardiac perfusion with 100 ml of 4% paraformaldehyde/0.1 M PB (pH 7.4). The entire GIT was carefully removed and divided into stomach, duodenum,

jejunum, ileum, and colon (Fig. 2B). The intestines were gently flushed to remove any contents and cut open longitudinally along the mesenteric line.

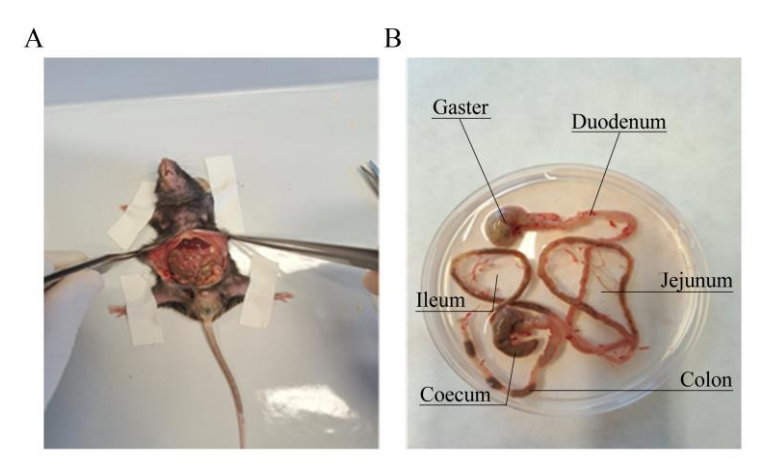


**Figure 2.** Preparation of the gastrointestinal tract for histological analysis. **A)** Opening of the peritoneal cavity **B)** Dissection of segments along the GIT employing the Swiss roll technique to facilitate the examination of the histological characteristics of the individual segments of the digestive tract.

The intestinal tissue was meticulously rolled with the mucosa facing outward using a wooden stick, a technique referred to as "Swiss roll" (Fig. 3), and fixed in 4% paraformaldehyde for a period of 24 hours. After fixation, the tissue samples were rinsed under running water, dehydrated through a graded ethanol series, cleared, and embedded in paraffin. Using a rotary microtome HistoCore BIOCUT (Leica Biosystems), 5 µm-thick sections were prepared and stained with hematoxylin and eosin following a routine protocol.

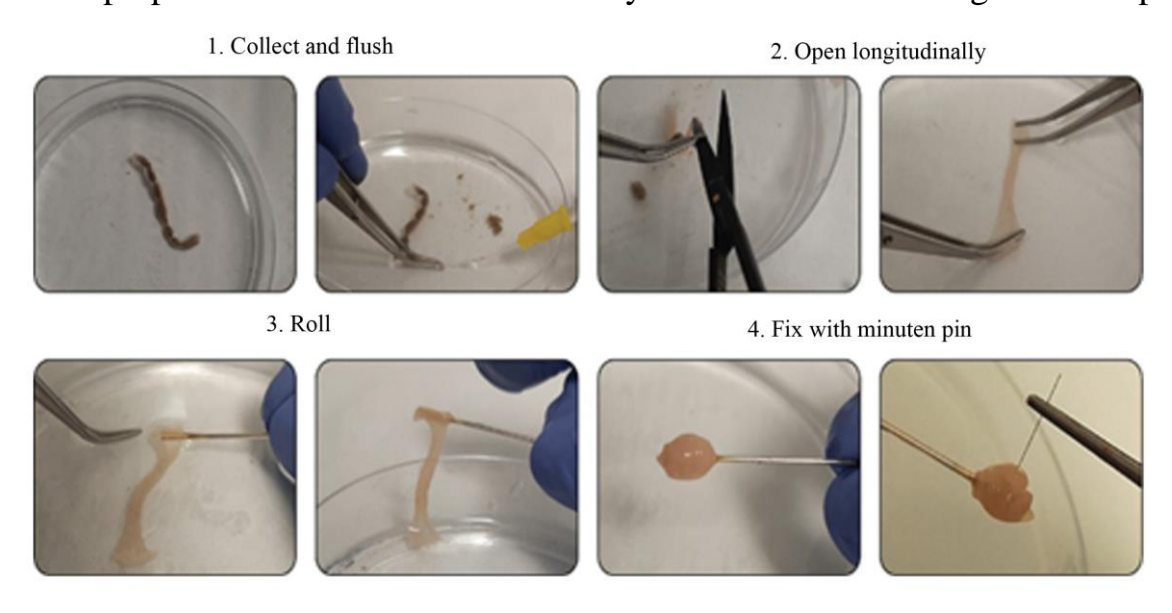


**Figure 3.** Workflow of the Swiss rolling technique for intestinal tissue. The four main sequential steps involved are depicted: 1 -The dissected segment is opened and cleared of contents; 2 -The lumen is opened with a longitudinal cut; 3 -The tissue is rolled with the mucosa facing outward; 4 -A needle is used to secure the rolled segment while removing the stick around which the tissue is rolled. The figure has been adapted from Le Naour et al.

# 3.2. Analysis and primer design for the splicing variants of the enzyme choline acetyltransferase

Using the Primer-BLAST program and in accordance with the recommendations published by Vanderbrouke II et al., forward and reverse primers were designed to target the M, N1, N2, R3, R4, pChAT, and cChAT mRNA splicing isoforms. The primer pairs used in the PCR analysis are listed in Table 1. All primers met the requirements of the default settings, which were modified as follows: melting temperature was calculated to be between 60 °C and 65 °C; GC content of 40% to 60%. Among all R isoforms, the R3 type is the only one containing exons Rb and Mb, so the primers' location was chosen to be in these unique exons (Fig. 4A). The forward primer for the R3 binds to a region within exon Rb, while the reverse primer hybridizes to a sequence in exon Mb. The R1 isoform contains exons Ra and Rb from the noncoding region of the gene. To detect this isoform, a forward primer in exon Rb and a reverse primer spanning the exon-exon junction of exons Rb and P1 were used. The R2 isoform contains only exon Ra from the noncoding region, and primer design suitable for its identification was unsuccessful. The R4 isoform contains exons Ra and Mb. For its detection, a forward primer hybridizing to the exon-exon junction and a reverse primer located in exon Mb were used (Fig. 4A). The N1 and N2 mRNA splicing isoforms are closely related, and the only difference between the two isoforms is the presence of exon Mb in the N1 isoform. A common forward primer located within exon N was used. The reverse primer for isoform N1 was chosen to bind to exon Mb, while the reverse primer for N2 isoform was specific to the splice junction between exon P1 and exon N. There were five base pairs at the 3' end of the primer overlapping with the adjacent exon (Exon P1\_N; Table 1, Fig. 4A). Similarly, for the pChAT isoform, that lacks all protein-coding exons from P5 to P8, the forward primer was located in exon P3, while the reverse primer targeted 5 base pairs within exon splice junction (Exon P9\_P4; Table 1, Fig. 4B). The forward primer used for amplification of the M splicing isoform was specific to a region within exon Ma, and the reverse primer was located in exon Mb. The primers used for amplification of the cChAT isoform were both located in exon 5.

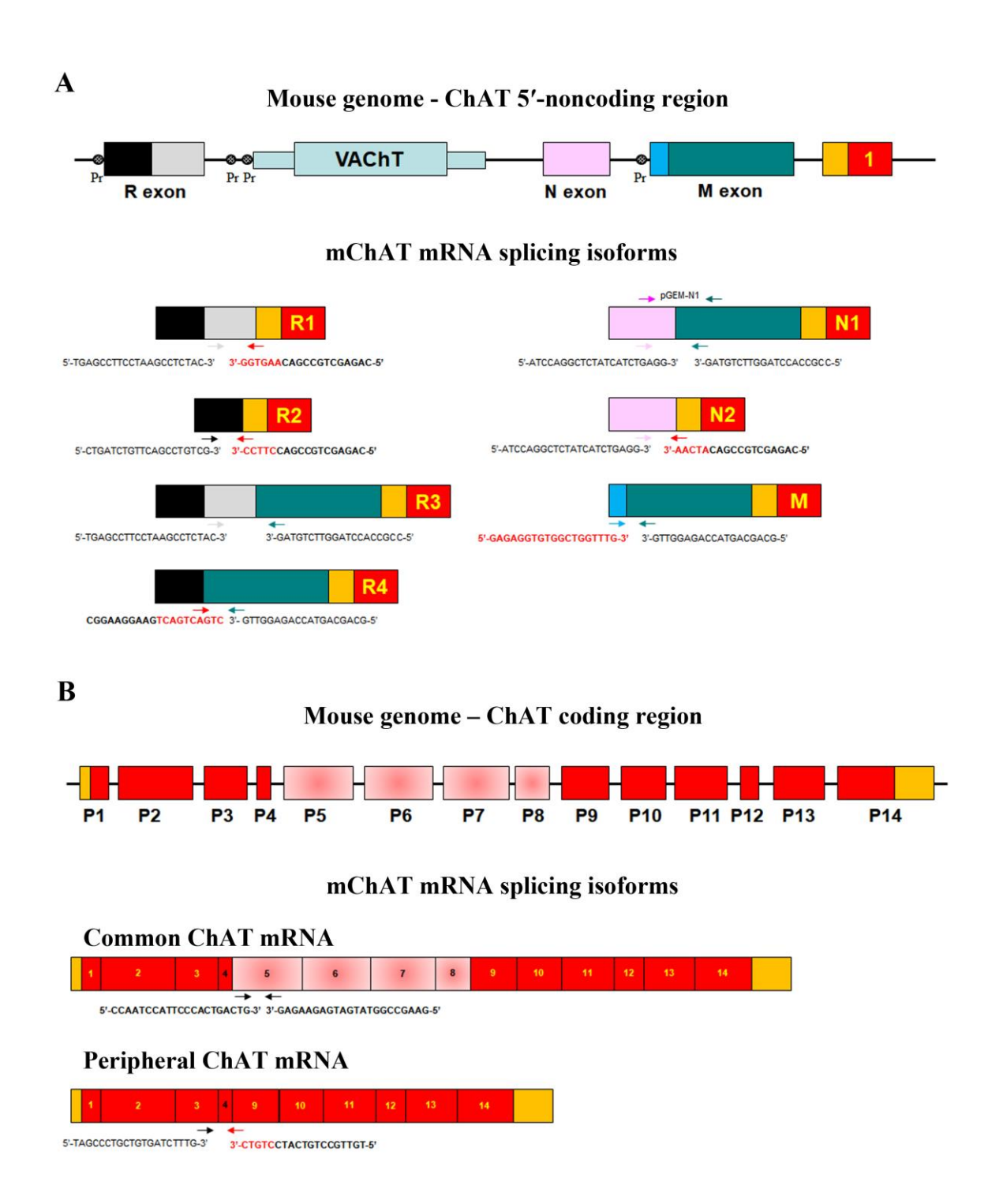


**Figure 4.** Schematic diagram showing the structure of the cholinergic gene locus and the splicing pattern of multiple mRNA isoforms of ChAT. A) Schematic representation of the gene structure encoding ChAT in mice and the seven splicing isoforms of its mRNA in the 5' untranslated region, with the positions of the specific primers indicated. **B**) Schematic representation of the two splicing isoforms of ChAT mRNA in the 3' coding region of the gene and the positions of the specific primers.

Lyophilized primers (Sigma-Aldrich, Germany) were initially resuspended in TE buffer (10 mM Tris, pH 8.0, 1 mM EDTA) to a concentration of 100 pmol/µl. The stocks were further diluted in TE buffer to a final concentration of 10 pmol/µl and stored at -20 °C.

Table 1. Sequence of primers used for PCR. The five base pairs, spanning the unique exon-exon junction

in the reverse primers for the N2, R1, and pChAT isoforms are shown in red.

mRNA for ChAT splicing isoforms (primer name)	Sequence 5` → 3`	Location of primers	Product length (bp)	Annealing temp. (t °C)
R3				
Forward (qRb Fwd)	TGAGCCTTCCTAAGCCTCTAC	Exon Rb	149	60
Reverse (qMb_Rev1)	CCGCCACCTAGGTTCTGTAG	Exon Mb		
N1				
Forward (qN_Fwd)	ATCCAGGCTCTATCATCTGAGG	Exon N	170	63
Reverse (qMb_Rev1)	CCGCCACCTAGGTTCTGTAG	Exon Mb		
N2				
Forward (qN_Fwd)	ATCCAGGCTCTATCATCTGAGG	Exon N	112	65
Reverse (qN2_Rev)	CAGAGCTGCCGAC <mark>ATCAA</mark>	Exon P1_N		
M				
Forward (qMa_Fwd)	GAGAGGTGTGGCTGGTTTG	Exon Ma	119	65
Reverse (qMb_Rev2)	GCAGCAGTACCAGAGGTTG	Exon Mb		
Peripheral ChAT				
Forward (qPC_Fwd)	TAGCCCTGCTGTGATCTTTG	Exon P3	125	65
Reverse (qPC_Rev)	TGTTGCCTGTCATCCTGTC	Exon P9_P4		
Common ChAT				
Forward (qCC_Fwd)	CCAATCCATTCCCACTGACTG	Exon P5	95	63
Reverse (qCC_Rev)	GAAGCCGGTATGATGAGAAGAG	Exon P5		
R1	TGAGCCTTCCTAAGCCTCTAC	Exon Rb		
Forward (qRb_Fwd)	CAGAGCTGCCGACAAGTGG		91	60/ 63
Reverse (qR1_Rev)	CAUAGCIGCCGACAAGIGG	Exon P1_Rb		
R4 Forward (qR4_Fwd) Reverse (qMb Rev2)	CGGAAGGAAGTCAGTC GCAGCAGTACCAGAGGTTG	Exon Ra_Mb Exon Mb	81	60/63

# 3.3. *De novo* design of double-stranded gBlock gene fragments and pGEM-N1 plasmid used in PCR reactions to test the specificity of isoform-specific primers

De novo designed double-stranded gBlock Gene fragments (Integrated DNA Technologies) and a plasmid pGEM-N1 Easy (Promega, Madison, WI) containing isoform-specific nucleotide sequences were used as templates. The gBlock-1 fragment contained the 5′-noncoding region of isoform R3 (exons Rb, Mb, P1, and part of P2) and a portion of exon P7, the entire P8 exon and part of exon P9 (Fig. 1A) from the coding region. It was used as a template to amplify the R3 isoform using primers qRb\_Fwd and qMb\_Rev1 (Fig. 1A). It was also used to check the specificity of the reverse primer (qN2\_Rev), encompassing the exon splice junction between exon P1 and N for the N2 isoform with primer qRb\_Fwd (expected product length of 280 bp, Fig. 1A). Similarly, gBlock-1 was used to check the specificity of the qPC\_Rev primer which was specific to the exon splice junction between exon P9 and exon P4 for isoform pChAT by combining it with qRb\_Fwd (expected product length of 618 bp, Fig. 4).

10	20	30	40	50 tcagcgtgtg	60	70
aggetgatet	geccageceg	ccycccycaa	accaggacgc	ccagegegeg	Cagcccccc	ggaaggaagg
80	90	100	110	120	130	140
qRb_Fwd						
TGAGCCTTCC	TAAGCCTCTA	Ctgacagcaa	agctgcagag	gccctgctgc	gtgagaccca	gaagcttcca
150	160	170	180	190	200	210
cgccactttc	agtcagtcgg	ggcggctgct	gggatctggc	aacttcgtcg	gaggctctgC	TACAGAACCT
						qMb_Rev1
220	230	240	250	260	270	280
AGGTGGCGGg	CCCAACCTCT	GGTACTGCTG	Ccacccctc	cctggccctt	ctggctcacg	cagccgcctc
	<					
qMb_Rev1	qMb_Rev2					
290	300	310	320	330	340	350
cagccctgct	tggtgtggaa	cagtgccggt	tcggtgcgta	acagcccagg	agagcagGTC	GGCAGCTCTG
					7.7.007	NO D
					AACTA	qN2_Rev
360	370	380	390	400	410	420
ctactctgga	ttaagaatcg	ctaggATGcc	tatcctggaa	aaggtccccc	caaagatgcc	tgtacaagct
430	440	450	460	470	480	490
tctagctgtg	aggaggtgct	ggacttacct	aagttgccag	tgcccccact	gcagcaaacc	ctggccacct
500	510	520	530	540	550	560
				cagcttgaat		
570	580	590	600	610	620	630
caagtccctg	cagtttgtgg	tgggccgaga	tggcacctgc	ggtgtggtgt	gtgagcactc	cccttttgat
640	650	660	670	680	690	700
ggcatcgtcc	tggtgcagtg	cacggagcac	ctgctgaaac	atatGATGAC	AGGCAACAag	aagctcgtc
				CTGTC	qPC Rev	

**Figure 5.** The sequence of the gBlock-1 fragment contained the 5'-noncoding region of isoform R3 (exons Rb, Mb, P1 and part of P2) and part of exon P7, the entire P8 exon and part of exon P9. The exact location of each forward and reverse primers is marked with an arrow. The 5 bases and the 3' end of the primers qN2\_Rev and qPC\_Rev encompassing the exon splice junction are also indicated.

The gBlock-2 fragment contained sequences specific for the N2, M, pChAT, and cChAT isoforms (Figure 6) and was used to test the corresponding primer pairs (Table 1).

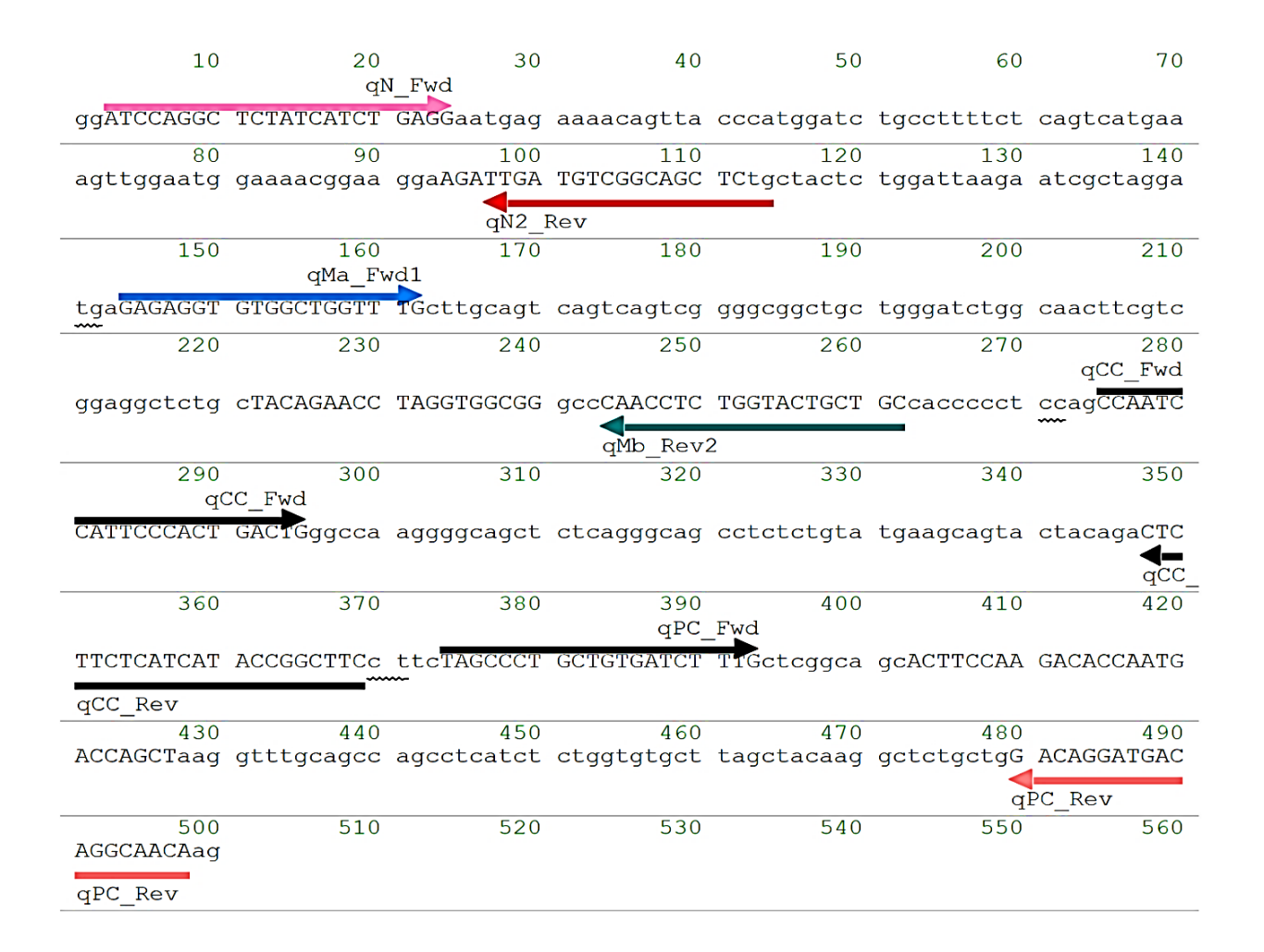


**Figure 6.** The sequence of the gBlock-2 fragment contained specific regions of the N2, M, pChAT, and cChAT isoforms. The exact location of each forward and reverse primers is marked with arrows.

Plasmid pGEM-N1, containing part of the 5'-noncoding region of the N1 isoform, was generated in a previous study and was used to test the specificity of primers amplifying the N1 isoform. Briefly, the amplified fragments were subcloned into the pGEM-T Easy plasmid vector (Promega, Madison, WI). A standard ligation reaction between the vector DNA and the insert DNA was performed. Transformation was carried out in *E. coli* Competent High DH5 cells (ZYMO RESEARCH), which were then cultured on agar plates containing 2% X-gal and ampicillin (50 mg/kg) at 37 °C overnight. The plasmid was purified using alkaline lysis.

### 3.4. Conventional polymerase chain reaction

PCR was carried out on a qTower<sup>3</sup> G Thermal Cycler (Analytik Jena, Germany). For the PCR,  $0.25~\mu\text{M}$  of forward and reverse primers,  $10~\mu\text{l}$  of 2x Luna Universal qPCR Master Mix (New England BioLabs, USA) and  $2~\mu\text{l}$  of template DNA (10~000 copies for gBlock-1 and gBlock-2, and  $20~pg/\mu\text{l}$  for pGEM-N1) were mixed with dH<sub>2</sub>O to a final volume of  $20~\mu\text{l}$ . PCR analysis allowed monitoring of the melting curves following amplification. When using

the reverse primers encompassing the exon splice junction (qN2\_Rev and qPC\_Rev), PCR conditions had to be optimized by adding 3% dimethyl sulfoxide (DMSO) to achieve improved specificity. DMSO stabilizes secondary DNA structures and prevents nonspecific primer annealing. The following PCR protocol was applied: initial denaturation at 95 °C for 60 seconds, followed by 40 cycles of 95 °C for 15 seconds; primer annealing at 60 °C, 63 °C, or 65 °C (specific for each primer pair) for 10 seconds; final extension at 60 °C for 30 seconds with fluorescence signal acquisition. After the last amplification cycle, melt curve analysis was performed over a temperature range of 60-95 °C. All PCR products were visualized on a 2% agarose gel stained with ethidium bromide to assess product quality and detect any potential nonspecific amplification. Hyper Ladder 25 bp (Bioline) was used as a DNA marker. Gel visualization was performed under UV light using an ultraviolet transilluminator (BIO View UST-20 M-8E, Biostep, Germany).

# 3.5. Construction of standard curves to determine amplification efficiency of each primer pair

To construct standard curves, serial dilutions of the gene fragments used as PCR template samples were prepared. Ten-fold serial dilutions of the double-stranded gBlock fragments were made, allowing the preparation of standards with a precisely defined number of molecules per template (ranging from  $1\times10^6$  to  $1\times10^2$ ). Each of these dilutions of gBlock-1, gBlock-2, and pGEM-N1 was used to generate standard curves via qPCR. Each standard was tested in duplicate, and the mean Ct value for each dilution was determined. The resulting data were used to generate a standard curve for each splicing isoform amplified using the corresponding template. The correlation coefficient (R<sup>2</sup>), the slope of each curve, and the amplification efficiency (E) were calculated for each standard curve.

### 3.6. Isolation of RNA from experimental animals

Five adult male C57Bl/6NCrl mice, aged 9–11 weeks, were used. During the experiment, animals were euthanized by intraperitoneal injection of Ketamine (100 mg/kg) and Xylazine (10 mg/kg), followed by careful dissection of the GIT organs. After opening the abdominal cavity, tissues from different parts of the digestive tract – stomach, duodenum, jejunum, ileum and colon – were collected. The samples were stored in RNase-inactivating buffer RNAlater (SIGMA) at -20 °C. Total RNA was extracted using the EXTRACTME Total RNA Kit (BLIRT S.A.). The kit provides a validated methodology for purifying RNA from biological material using column extraction membranes. Homogenization with the bead-beating tubes provided in the kit proved unsatisfactory, so a Cole-Parmer SamplePrep HG-400 MiniG Tissue Homogenizer and Cell Lyser (Cole-Parmer, USA) was used to completely homogenize the material. Isolation of total RNA from tissues was performed according to the manufacturer's protocol (Appendix 2).

The concentration and purity of the isolated total RNA from mouse stomach, duodenum, jejunum, ileum, and colon were determined using a spectrophotometer (NanoDrop One, Thermo Scientific) (Table 2). For this purpose, 2  $\mu$ l of each sample and 2  $\mu$ l of RNase-free water for instrument blanking were used. The optical density of the solution was measured at 260 nm (A260) and 280 nm (A280). The RNA purity coefficient (K) was determined as K = A260/A280. The measured ratio ranged between 1.8 and 2.0, indicating that the isolated RNA from stomach, duodenum, jejunum, ileum, and colon was of sufficient quality for subsequent complementary DNA synthesis and quantitative analysis.

**Table 2.** Concentration and purity of isolated RNA from the stomach, duodenum, jejunum, ileum, and colon as determined by spectrophotometry.

Laboratory animal	GIT segment	Quantity of isolated RNA	A260/A280 ratio
	Gaster	111,90 ng/μl	1,99
	Duodenum	1240,80 ng/μl	2,05
Mouse 1	Jejunum	513,60 ng/μl	2,11
	Ileum	307 ng/μl	2,12
	Colon	103,7 ng/ μl	1,9
	Gaster	78,8 ng/μl	2,08
	Duodenum	180,3 ng/μl	2,06
Mouse 2	Jejunum	72 ng/μl	2,02
	Ileum	67,7 ng/μl	1,80
	Colon	45,0 ng/μl	1,97
	Gaster	493 ng/μl	2,16
	Duodenum	235,3 ng/μl	2,15
Mouse 3	Jejunum	399,7 ng/μl	2,11
	Ileum	83,2 ng/μl	2,16
	Colon	20,5 ng/μl	1,93
	Gaster	369 ng/μl	1,95
	Duodenum	428,9 ng/μl	2,00
Mouse 4	Jejunum	239,2 ng/µl	1,97
	Ileum	135,6 ng/μl	1,87
	Colon	98,9 ng/μl	2,01
Mouse 5	Gaster	302,6 ng/μl	2,11
	Duodenum	609,4 ng/μl	2,03
	Jejunum	564,7 ng/μl	2,10
	Ileum	265,6 ng/μl	2,09
	Colon	663,5 ng/μl	2,20

# 3.7. Synthesis of complementary DNA (cDNA)

Complementary DNA (cDNA) was synthesized from the isolated total RNA using the TRANSCRIPTME RNA Kit. The reaction mixture contained 1  $\mu g$  of total RNA, 10  $\mu L$  of 2x RT Master Mix, 2  $\mu L$  of TRANSCRIPTME Enzyme Mix, and DEPC-treated water, for a final volume of 20  $\mu L$ . The mixture was incubated at 25 °C for 10 minutes, then at 50 °C for 30 minutes. Finally, the reverse transcriptase was inactivated by incubating the mixture at 85 °C for 5 minutes. To degrade any residual RNA, 1  $\mu L$  of RNase H was added to the reaction mixture. The resulting cDNA was diluted 1/50 and used as a template for quantitative analysis.

# 3.8. Quantitative PCR using specific primer pairs and cDNA from the stomach, duodenum, jejunum, ileum, and colon of C57BL/6NCrl mice

Quantitative PCR with specific primer pairs and corresponding cDNA from different parts of the GIT was performed according to the following protocol presented in Table 3.

**Table 3.** Components and conditions of qPCR with cDNA from stomach, duodenum, jejunum, ileum and colon of C57Bl/6NCrl mice.

Component reaction m		Stage of the qPCR reaction	Temperature	Timing and repeatability of the cycle	
Luna qPCR	10µl	initial denaturation	95 °C	60 sec	
Forward prim	er	denaturation	95 °C	15 sec	
Reverse prim 0,5µl	er	Aniyling (variant specific)	60 °C , 63 °C, 65°C	10 sec	40 cycles
cDNA	2 μ1	elongation		30 sec	
dH <sub>2</sub> O	7 μl	melt curve analysis	60-95 °C		·
Final volume	20µl				

Prepare the reaction mixture (Master mix) by first adding dH<sub>2</sub>O to the tube, followed by the isoform-specific primer pair, DMSO (for the N2 and pChAT isoforms), and finally the Luna Universal qPCR Master Mix. The prepared Master mix is then vortexed using a Vortex V-1 plus (Biosan, Latvia) for 5–10 seconds and briefly centrifuged using a Centrifuge-Vortex CVP-2 (Biosan, Latvia) at 1200 rpm. Each of the studied splicing isoforms – R3, N1, N2, M, pChAT, and cChAT – in the respective material from the different parts of the GIT is analyzed simultaneously in three wells. To avoid false-positive results in the qPCR analysis, negative controls (lacking cDNA) were included for each splicing isoform, added in triplicate. In order to relatively quantify the isoforms in the digestive tract of C57Bl/6NCrl mice, an experiment was conducted for comparative analysis of gene expression using the

ΔΔCt method, modified according to Pfafl's method, taking into account the actual efficiency of the reaction for each isoform. For each isoform, the change in expression (fold change) in the stomach, small intestine, and large intestine was calculated. In order to perform the analysis correctly, the expression of the reference gene glyceraldehyde-3-phosphate dehydrogenase (GAPDH) was also examined. A pair of primers, presented in Table 4, was used for the amplification of GAPDH.

**Table 4.** Forward (Fwd1) and reverse primer (Rev1) used for GAPDH amplification in the course of qPCR.

Primers	Nucleotide sequence 5`→3`	Product length (bp)
mGAPDH_Fwd1	AGGTCGGTGTGAACGGATTTG	21
mGAPDH_Rev1	TGTAGACCATGTAGTTGAGGTCA	23

### 3.9. Statistical analysis

All data from the qPCR experiments of the splicing isoforms examined are presented as the mean  $\pm$  standard error of the mean (SEM) of the five animals examined. Statistical analysis was performed with SigmaPlot 11 (Systat Software, USA). One-factor analysis of variance (One-Way ANOVA) was used to compare the expression of individual isoforms. When the assumptions of equal variance (Equal Variance) and normal distribution (Normality) were not met, expression differences were assessed by ANOVA on Ranks and Kruskal-Wallis One-Way ANOVA on Ranks. Results were considered statistically significant at p  $\leq$  0.05. One-factor analysis of variance (One-way ANOVA) was applied to statistically analyze the expression of M, cChAT and pChAT in individual organs, followed by Tukey's multiple post-hoc test to assess statistically significant differences between isoforms within each organ relative to the stomach. Results were considered statistically significant at p  $\leq$  0.05.

### **III. Results**

### 1. Histological organization of the wall of the digestive tract of C57Bl/6NCrl mice

To demonstrate the normal morphology of the wall of the mouse GIT, the Swiss roll histological technique is used, followed by hematoxylin and eosin (H&E) staining (Fig. 7. A, B).

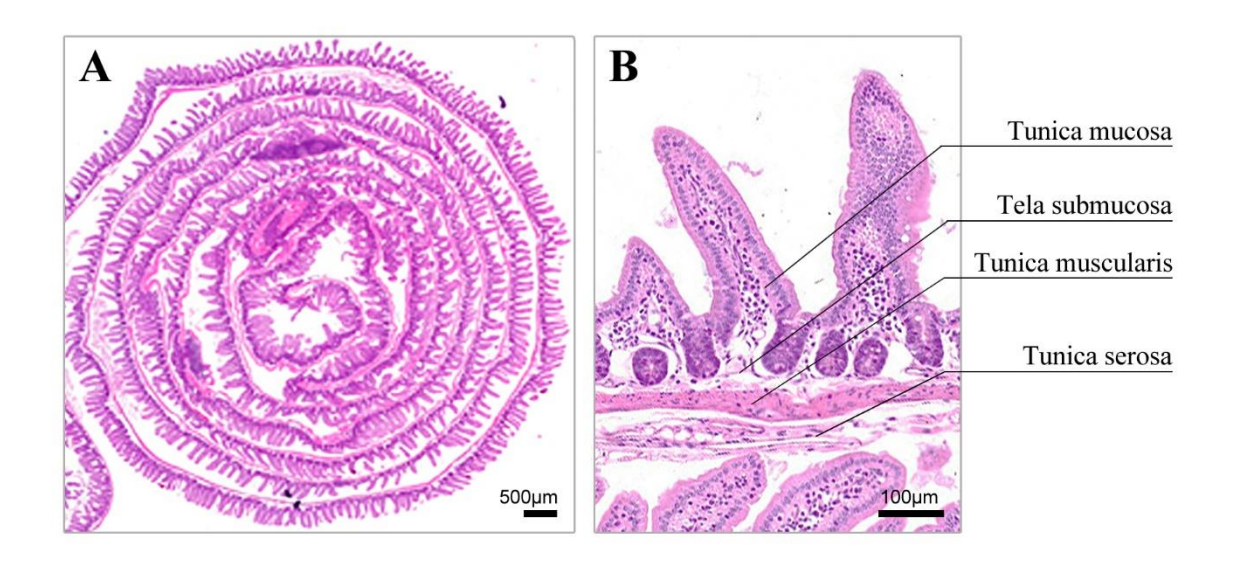
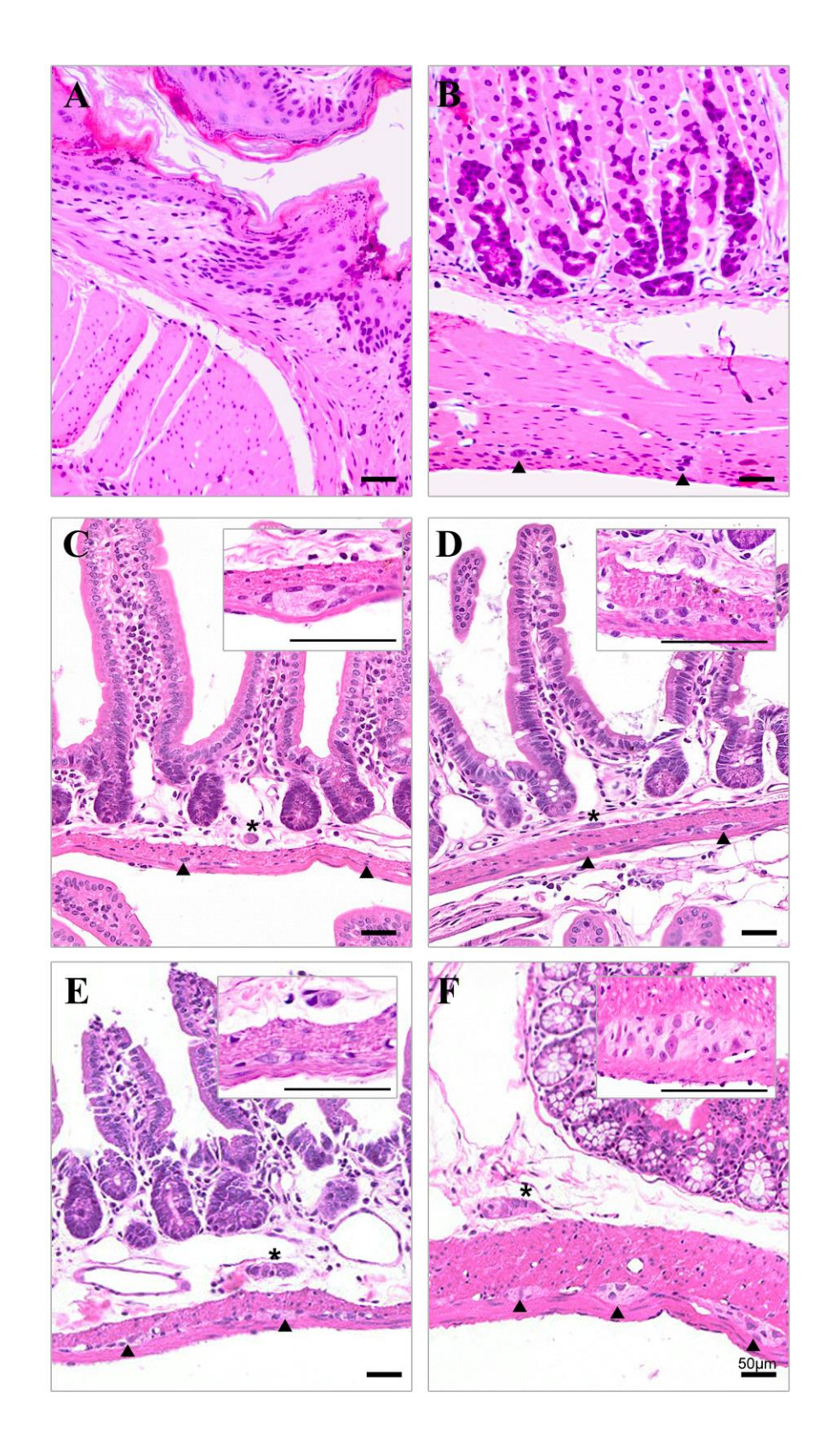


Figure 7. Representative images of H&E staining of small intestine Swiss-rolls. A) H&E staining of Swiss roll section from the small intestine of C57Bl/6NCrl mice  $\bf B$ ) Principal organization of the intestinal wall. Scale bar = 500 and 100 $\mu$ m.

The innermost layer of the digestive tract is represented by the mucosal layer, *tunica mucosa*, and its associated exocrine glands. Beneath the mucosa lies the less prominently stained submucosal layer, *tela submucosa*. Within this layer is the submucosal enteric plexus, *plexus submucosus*, composed of ganglia and neural structures surrounded by the connective tissue of the submucosa. The prominence of the submucosal plexus varies along different regions of the digestive tract, being most clearly observed in the small intestine (Fig. 8B-D). Next are the strongly eosinophilic smooth muscle fibers of the *tunica muscularis*, organized into an inner and outer layer. Between these two layers lies the myenteric (Auerbach's) plexus, *plexus myentericus* (Fig. 8B–E), consisting of well-defined ganglia and interconnected neural structures. Each ganglion contains several neurons. Individual neurons exhibit strongly basophilic nuclei, often containing one or more nucleoli.



**Figure 8.** H&E staining of Swiss roll sections from different parts of the GIT of C57Bl/6NCrl mice. The forestomach ( $\mathbf{A}$ ); stomach proper ( $\mathbf{B}$ ); duodenum ( $\mathbf{C}$ ); jejunum ( $\mathbf{D}$ ); ileum ( $\mathbf{E}$ ) and colon ( $\mathbf{F}$ ) are visualized. Ganglia of plexus myentericus (arrowhead) and plexus submucosus (star) are observed. Scale bar = 50  $\mu$ m.

At the periphery of the ganglia, small glial cells are located around the neurons (Fig. 8A and B). On most of the histological sections, connective tissue sheath around the ganglia is not observed. Along with the oval-shaped ganglia, those with highly elongated margins are also observed.

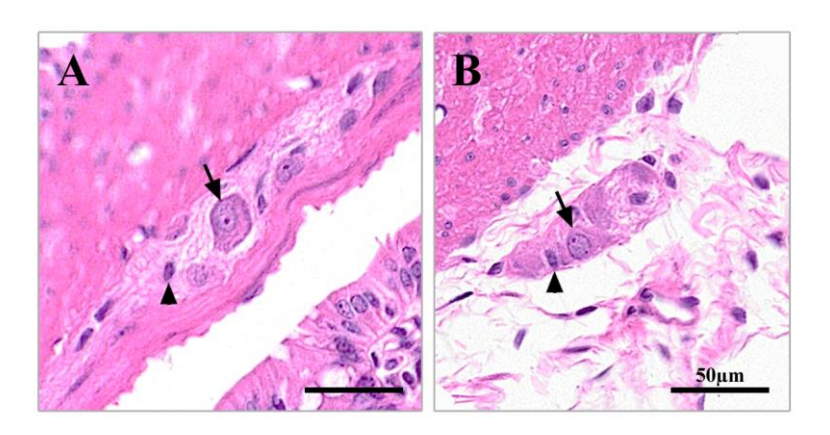


**Figure 9.** H&E staining of Swiss roll sections from the colon of C57Bl/6NCrl mice. **A)** enteric neurons (indicated by arrows) and glial cells (indicated by arrowhead) are observed within the plexus myentericus **B)** plexus submucosus with enteric neurons and glial cells located within it. Scale bar =  $50 \mu m$ .

# 2. Testing the specificity of *de novo* synthesized primer pairs and DNA templates in conventional real-time PCR

De novo designed double-stranded gBlock Gene Fragments – gBlock-1, gBlock-2, and plasmid pGEM-N1 containing isoform-specific nucleotide sequences were used as templates. The pGEM-N1 plasmid was used to test the specificity of primers amplifying the N1 isoform. The gBlock-1 fragment was used in control reactions to demonstrate the specificity of the reverse and boundary spanning primers used to amplify the R1, R4 (Fig. 10), and N2 isoforms (Fig. 12B). The R3 isoform was also amplified using the gBlock-1 template. The gBlock-2 fragment was used to test the specificity of primer pairs for the N2, M, pChAT and cChAT isoforms. Using the designed isoform-specific primers and the corresponding templates, the expected size fragments for R3 (149 bp), N1 (170 bp), N2 (112 bp), M (119 bp), pChAT (125 bp) and cChAT (95 bp) isoforms of ChAT mRNA were amplified using PCR. It was possible to design unique primer pairs for the R3, N1, M and cChAT mRNA isoforms because they have at least one unique exon. The R1 isoform shows high homology to the R3 splice isoform. For its identification, the forward primer qRb\_Fwd1 and the reverse primer qR1\_Rev were used (Fig. 4A). The forward primer is common to both isoforms, while the reverse one is specific to R1. To test the specificity of the reverse primer, a control reaction was performed with gBlock-1. With primer specificity for the R1 variant, no amplification was expected in the corresponding reaction. With the product available, its expected length was 280 bp. Nonspecific amplification products were obtained at 60 °C, demonstrating the nonspecificity

of the reverse primer used. After increasing the temperature to 63 °C the result remained the same. Control reaction results were visualised by gel electrophoresis (Fig. 4A, Fig. 10). In the R3, the forward primer qRb\_Fwd binds to a region of the Rb exon that is unique to this splicing isoform. As a reverse primer, qMb\_Rev1 was used, hybridizing to a sequence in the Mb exon. For the R4, a specific forward primer qR4\_Fwd was used, hybridizing in the exon binding region between the Ra and Mb exons. As a reverse primer, qMb\_Rev1 was used, hybridizing in the Mb exon (Fig. 4A). The R4 isoform demonstrated high homology to the R3, N1, and M. For its validation, control reactions were also performed with the respective templates – gBlock-1, pGEM-N1 and gBlock-2. With the specificity of the forward primer, no amplification product was expected in the respective reactions. Amplification products of 81 bp length were observed in the three control reactions and confirmed by gel electrophoresis (Fig. 10). Raising the hybridization temperature did not produce an optimal result during PCR amplification, demonstrating the nonspecificity of the forward primer and its inability to be used to identify the R4 isoform.

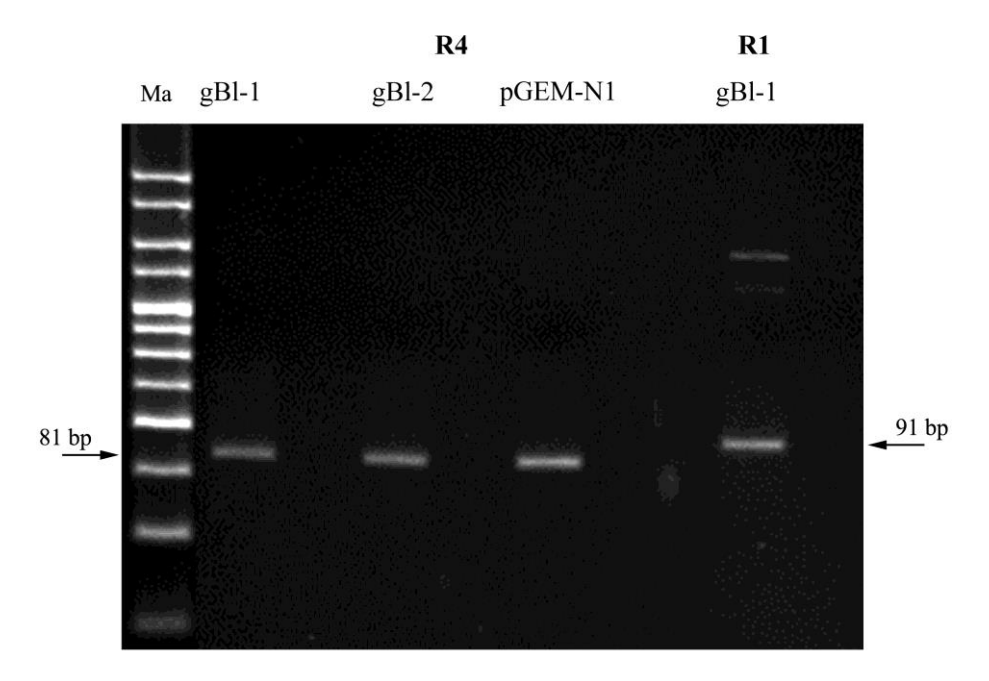


**Figure 10**. Gel electrophoresis of control primer pair amplification reactions for isoform R4 with gBlock-1, gBlock-2 and pGEM-N1 arrays confirming no specificity of primers used. Control reaction to test the specificity of the reverse primer for R1 with the gBlock-1 template at 60 °C demonstrating nonspecific amplification products. HyperLadder<sup>TM</sup> 25 bp (Bioline) was used as a molecular marker.

The forward primer used to detect both the N1 and N2 isoforms was common and located in exon N. The reverse primer for isoform N1 is qMb\_Rev, which was chosen to bind to exon Mb. The lack of unique exons in the N2 and pChAT isoforms necessitated the use of boundary spanning primers with 5 base pairs crossing the unique exon-exon junctions of these isoforms. The reverse primer for the N2 isoform encompassed the exon splice junction of exon P1 and exon N (Exon P1\_N). Five base pairs overlapping exon N are located at the 3'-

end of this primer. The forward primer used for amplification of the M isoform is qMa\_Fwd, and is located in the exon Ma. The reverse primer is qMb\_Rev2, and is located in the Mb exon. The primers used for amplification of cChAT are qCC\_Fwd and qCC\_Rev. Both primers are located in exon 5, which is unique to this isoform. For pChAT, which lacks the coding exons from P5 to P8, the forward primer qPC\_Fwd is located in exon P3. The reverse primer qPC\_Rev, similar to the N2 isoform, encompassed with 5 base pairs the exon splice junction between exon P4 and exon P9 (Exon P9\_P4). The gBlock-1 was reused in a control PCR reaction to verify the specificity of these reverse primers hybridizing to the exon splice junctions. The qRb\_Fwd was used as the forward primer in both reactions.

The appropriate annealing temperature which yields sufficient specificity for each tested primer pair was as follows: R3 - 60 °C; N1 - 63 °C; N2 - 65 °C; M - 65 °C; cChAT- 63 °C and pChAT - 65 °C. The optimal annealing temperature is the range of temperatures where efficiency of PCR amplification is maximal without nonspecific products. Optimization of primer annealing involves lowering the reaction temperature to make it possible for the primers to bind to their complementary DNA. The optimal annealing temperature depends on the PCR results. In the case of lack of amplification or a low quantity of amplified product, the annealing temperature should be lowered in increments of 2-3 °C. When nonspecific amplification products exist, the annealing temperature should be raised in increments 2-3 °C. Due to the high homology at the 3′ end of exon N and Mb for the isoform N2, as well as exon P4 and P8 for pChAT, the annealing temperature had to be increased to 65 °C. This temperature resulted in a lack of nonspecific amplification in the control reaction with primer qRb\_Fwd and gBlock-1 as a template, as detected on 2% agarose gel (Fig. 12B).

Analysis of denaturation curves was used to test the specificity of the amplification products obtained. After the final cycle of denaturation, primer annealing, and extension of the daughter DNA strand, melting curve analysis was performed in the temperature range of 60-95 °C. The number of peaks and the melting temperature were recorded for the curve of each positive sample. Analysis of melting curves from PCR experiments demonstrated the high specificity of amplification obtained with the *de novo* synthesized primer pairs, which were used for subsequent analysis of ChAT mRNA isoforms in the mouse GIT. A distinct peak was observed in the melting curves for all isoforms, clearly indicating the specificity of the resulting amplicons (Fig. 11).

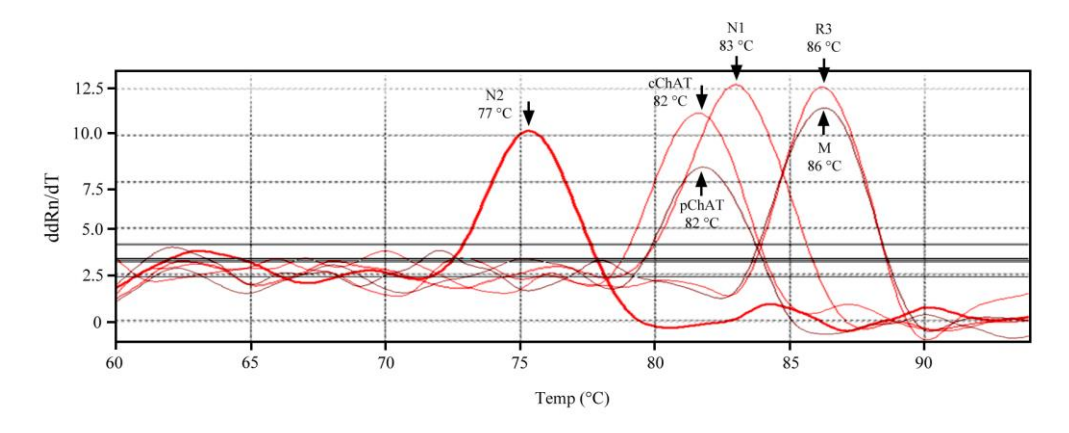


*Figure 11. Melt curve analysis of the amplification products of the PCR reaction with the de novo synthesized primer pairs and DNA fragments.* 

The absence of additional nonspecific products was confirmed by visualization on a 2% agarose gel stained with ethidium bromide (Fig. 12A). During real-time amplification, control reactions containing gBlock-1 exhibited a gradual increase in fluorescence signal during the final cycles, and melt curve analysis revealed a minor secondary peak in addition to the expected one. This indicated some nonspecific primer binding. To achieve the desired specificity, 3% DMSO was added to these reactions, which resulted in complete specificity without affecting amplification efficiency (Fig. 12B).

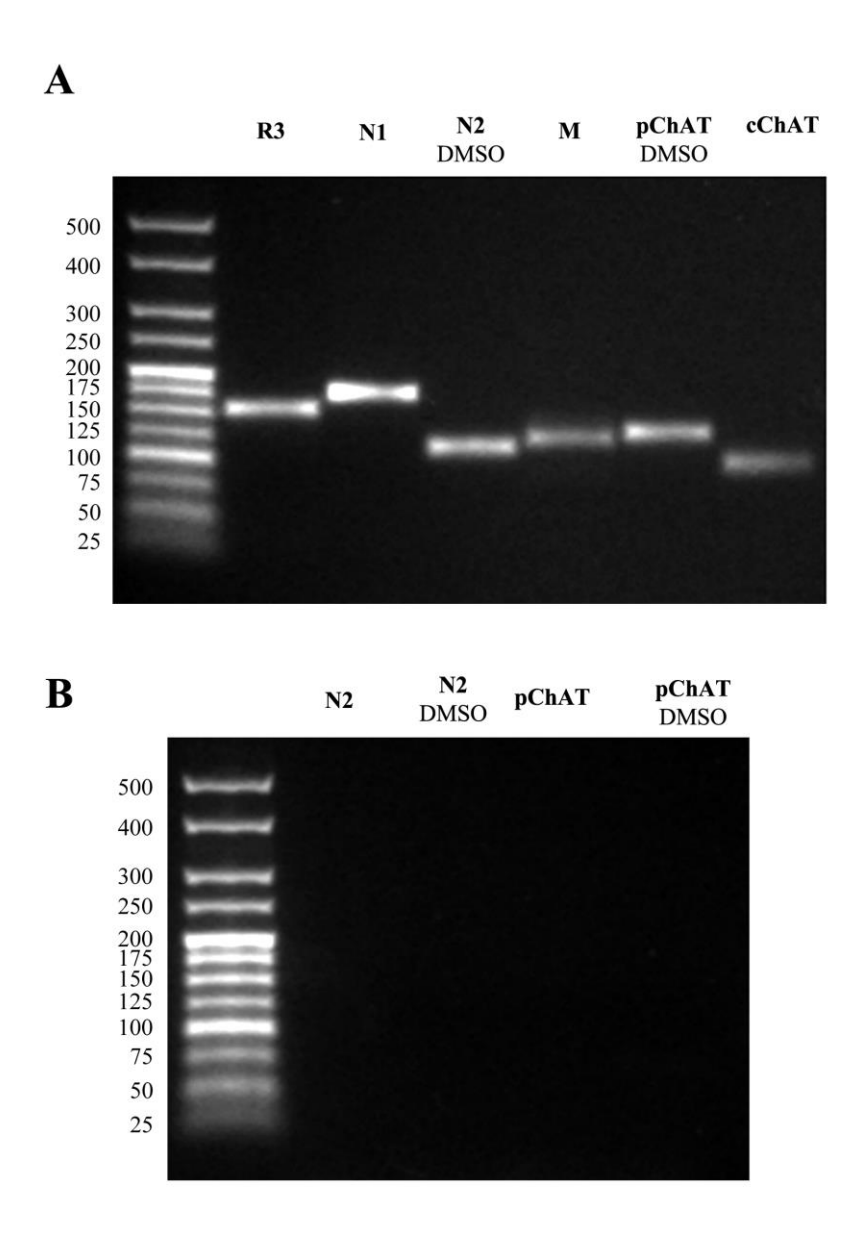


**Figure 12.** A) Gel electrophoresis of amplified fragments with expected size of R3 (149 bp), N1 (170 bp), N2 (112 bp), M (119 bp), pChAT (125 bp), and cChAT (95 bp) isoforms of ChAT mRNA using the isoform-specific primers and the corresponding templates (gBlock-1 for the R3 isoform; gBlock-2 for the N2, M, pChAT and cChAT isoforms, pGEM-N1 for the N1 isoform. **B**) Gel electrophoresis of control reaction of amplification with primer qRb-Fwd, isoform-specific reverse primers for N2 and pChAT and gBlock-1 as a template, with or without DMSO.Ma, DNA ladder marker HyperLadder<sup>TM</sup> 25 bp (Bioline); DMSO, dimethyl sulfoxide.

### 3. Relative quantitative analysis of the expression of ChAT mRNA isoforms

### 3.1. Generation of standard curves

Each of the serial 1/10 dilution of the templates (gBlock-1, gBlock-2, and pGEM-N1) was used to generate standard curves by qPCR. Each standard was run in duplicate, and the mean Ct value for each dilution was determined. Throughout the PCR reactions, the resulting amplification and melting curves were analyzed (Figs. 13–18).

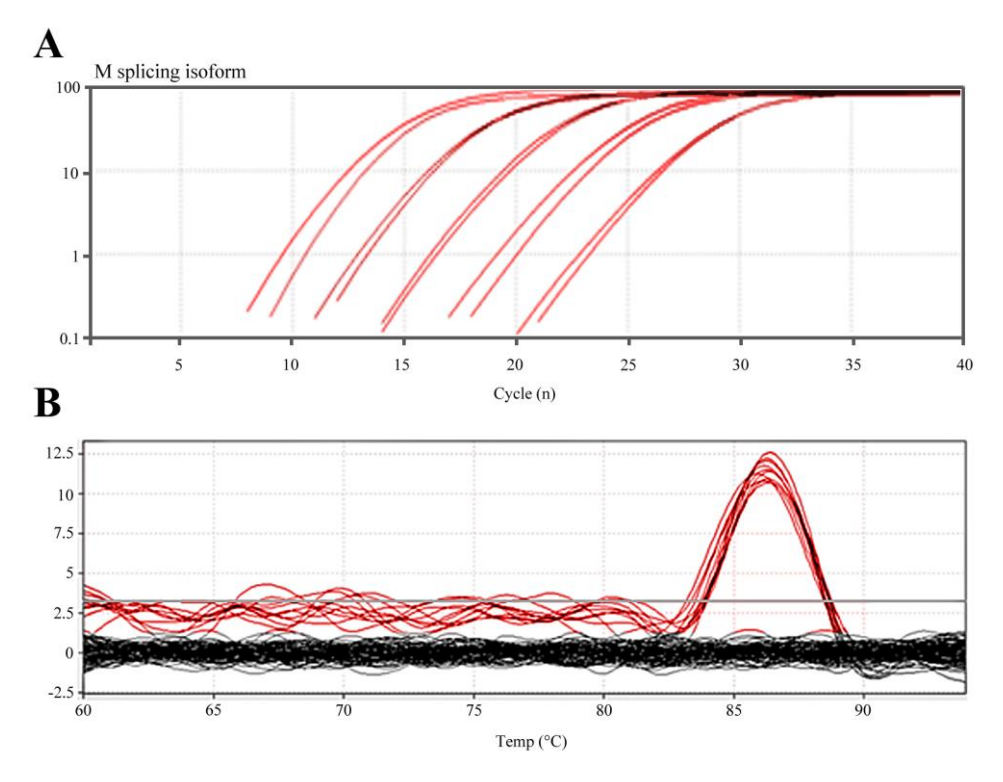


**Figure 13. A)** Amplification curve and **B)** denaturation curve of M isoform, demonstrating specific amplicons and denaturation peaks at 86  $^{\circ}$ C.

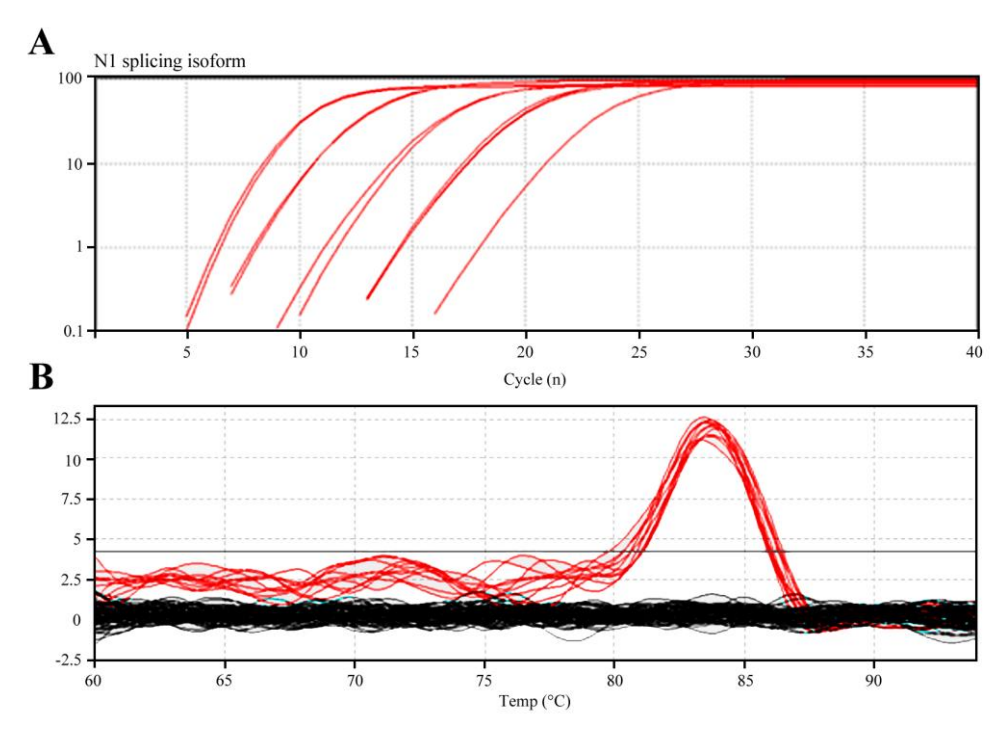


**Figure 14.** A) Amplification curve and B) denaturation curve of N1 isoform, demonstrating specific amplicons and denaturation peaks at 83 °C.

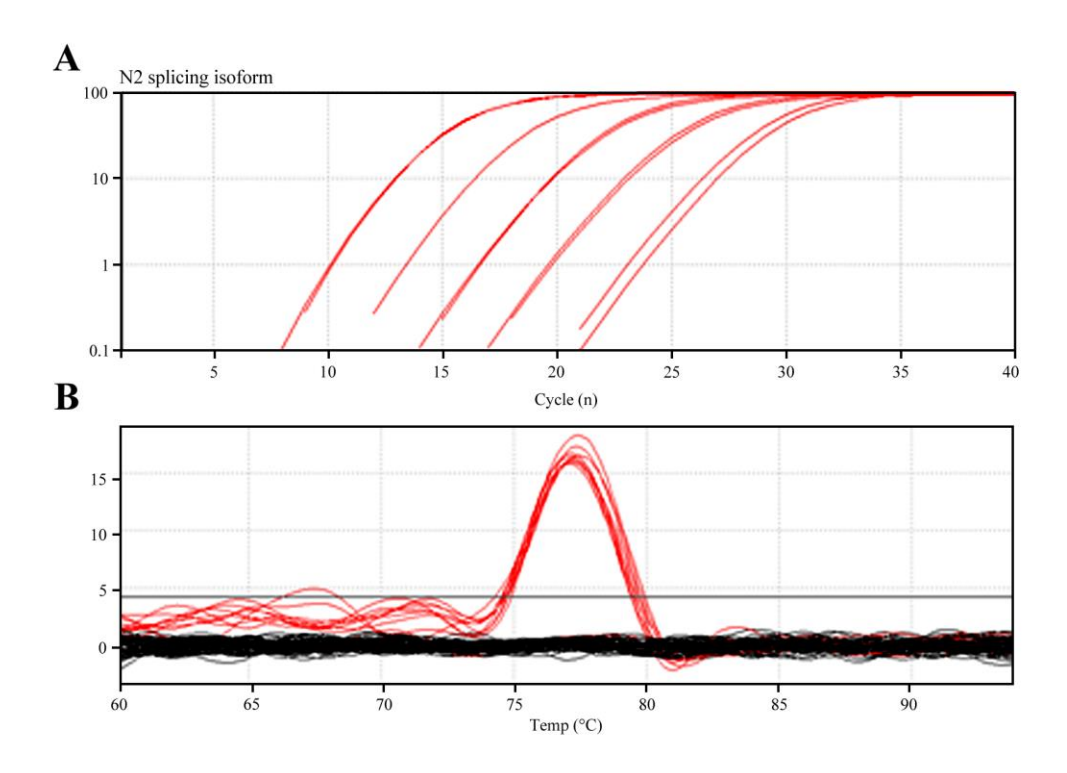


**Figure 15.** A) Amplification curve and (B) denaturation curve of N2 isoform, demonstrating specific amplicons and denaturation peaks at 77 °C.

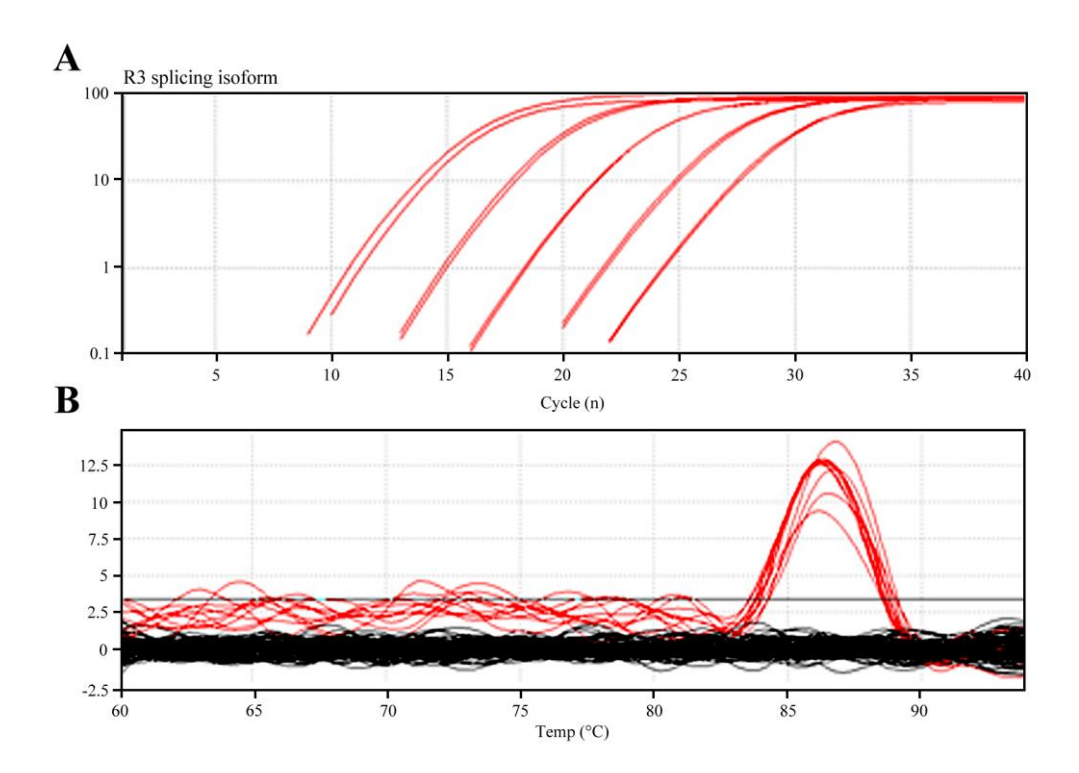
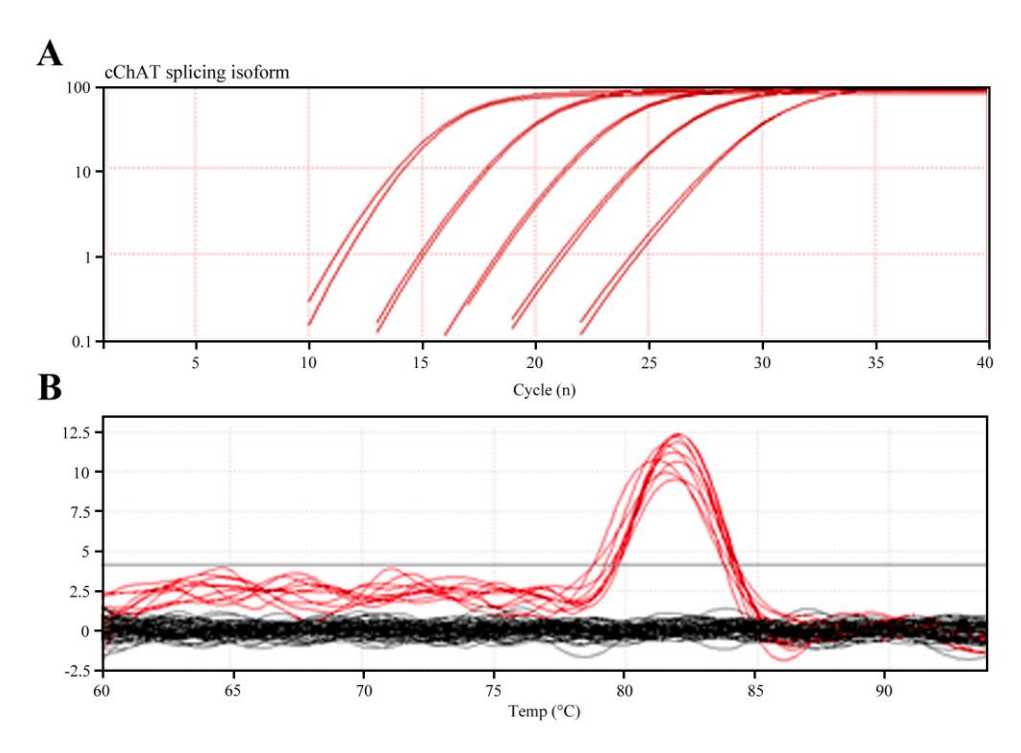


Figure 16. A) Amplification curve and B) denaturation curve of R3 isoform, demonstrating specific amplicons and denaturation peaks at 86 °C.



**Figure 17.** A) Amplification curve and **B**) denaturation curve of cChAT isoform, demonstrating specific amplicons and denaturation peaks at 82 °C.

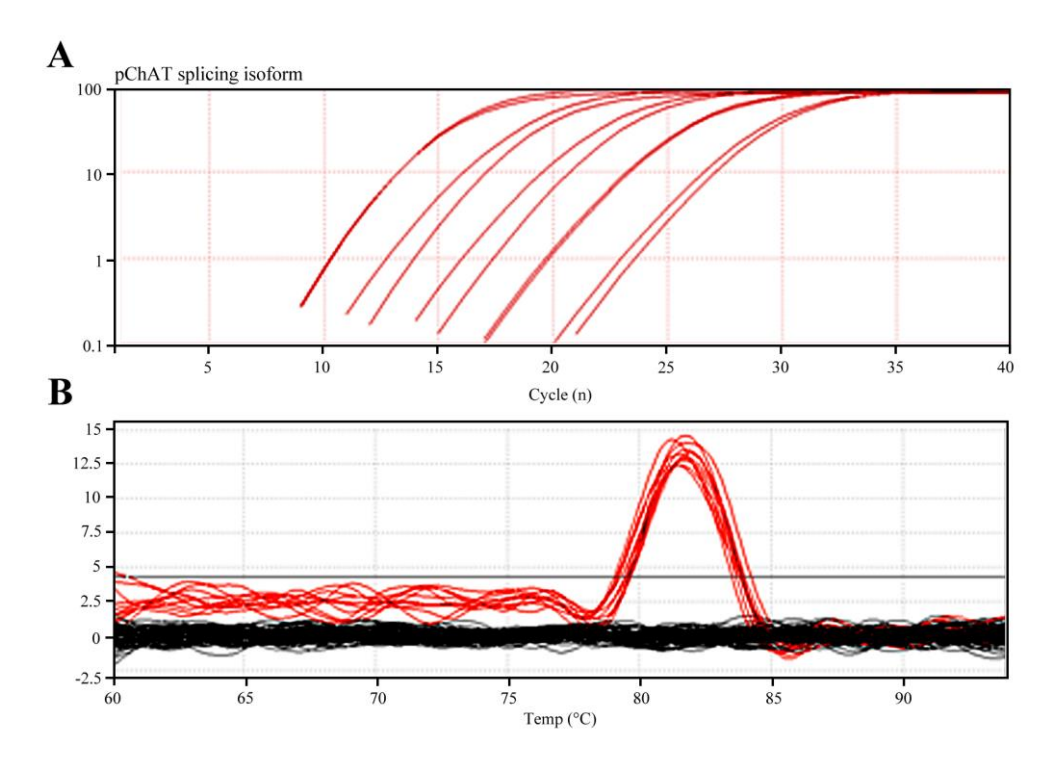


Figure 18. A) Amplification curve and B) denaturation curve of pChAT isoform, demonstrating specific amplicons and denaturation peaks at 82  $^{\circ}$ C.

# 3.2. Determination of the amplification efficiency of each primer pair

The results from quantitative PCR with diluted DNA fragments were used to generate a standard curve for each ChAT mRNA isoform. For each curve, the slope, correlation coefficient (R<sup>2</sup>), and reaction efficiency were calculated (Table 5). The slope of the standard curve in real-time PCR was used to determine the amplification efficiency, with values between -3.1 and -3.6 corresponding to efficiencies between 90-110%, which is considered the optimal range in qPCR analysis. The standard curve was graphically represented as a semi-logarithmic regression line of the Ct value against the logarithm of the corresponding isoform. The response efficiency was determined using the formula  $E = (10^{-1/\text{slope}} - 1) \times 100$ . One hundred percent reaction efficiency was obtained with a 10-fold increase in PCR product every 3.32 cycles during the exponential amplification phase (log 2<sup>10</sup>=3,3219). A standard curve with a slope of -3.32 indicates 100% PCR reaction efficiency. Another important characteristic of the standard curve is the correlation coefficient (R2), which indicates how well the data fit the regression line. The R<sup>2</sup> value reflects the linearity of the standard curve. The generation of standard curves for the ChAT isoforms yielded high correlation coefficients, and the efficiency of the PCR reactions ranged from 96.8% to 109.3% (Figs. 19A-F). The efficiency of the primer pair amplifying the GAPDH reference gene was previously determined to be 99% at hybridization temperatures of 60, 63, and 65 °C.

**Table 5:** Characteristics of the generated standard curves.

Splicing isoforms	Slope	Correlation coefficient (R <sup>2</sup> )	PCR efficiency (E)
M	-3,331	0,9998	99. 6%
N1	-3,118	0,0028	109. 3%
N2	-3,363	0,9994	98. 3%
R3	-3,4	0,9954	96. 8%
cChAT	-3,322	0,9983	99. 6%
pChAT	-3,332	0,9995	100%

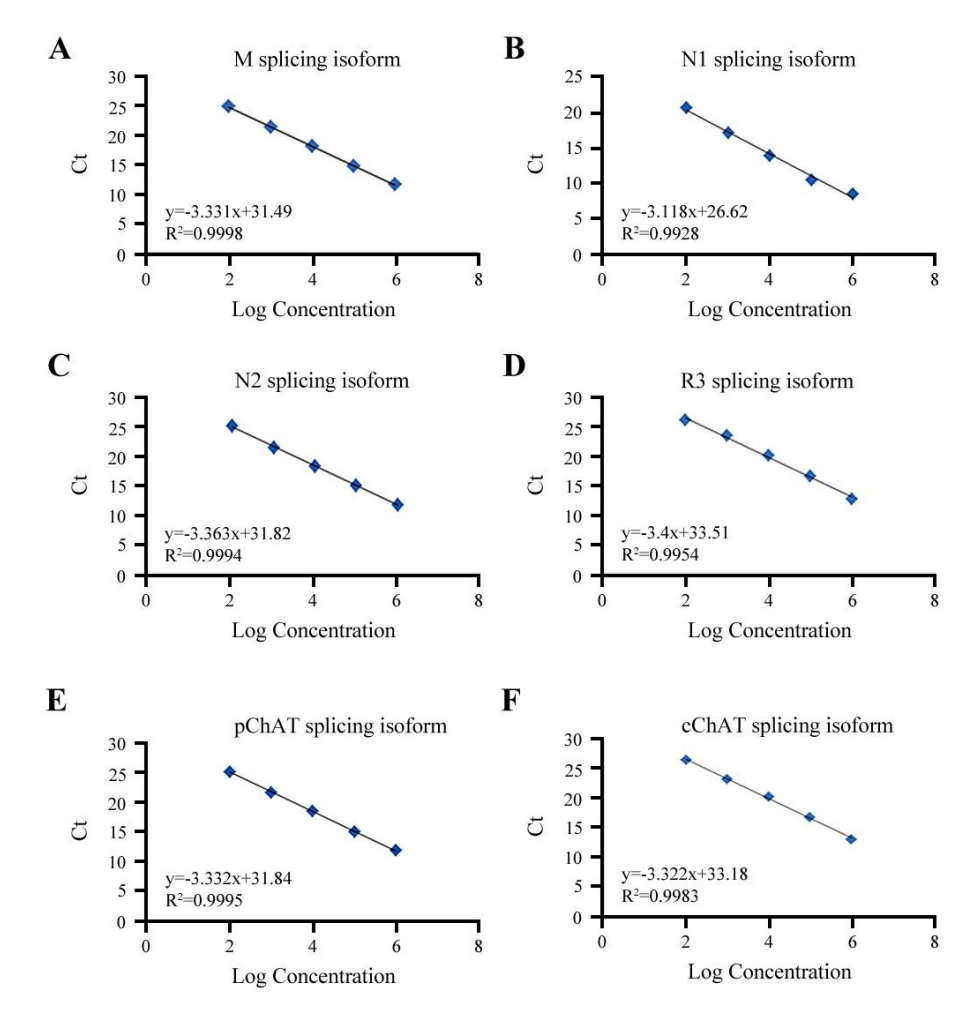


**Figure 19.** (A) Standard curve of the M isoform with a reaction efficiency of 99.6%; (B) standard curve of the N1 isoform with a reaction efficiency of 109.3%; (C) standard curve of the N2 isoform with a reaction efficiency of 98.3%; (D) standard curve of the R3 isoform with a reaction efficiency of 96.8%; (E) standard curve of the pChAT isoform with a reaction efficiency of 99.6%; and (F) standard curve of the cChAT isoform with a reaction efficiency of 100%.

# 3.3. Expression of ChAT isoforms across mouse gastrointestinal tract via real-time PCR

For the isoforms successfully amplified using DNA templates, amplification products and melting curves were analyzed during qPCR using cDNA from the experimental mouse tissues. The analysis demonstrated high specificity of amplification obtained with the *de novo* synthesized primer pairs for the M, cChAT and pChAT isoforms and the corresponding cDNA (Figs. 20, 21, 22A). In the stomach, duodenum, jejunum, ileum, and colon of C57Bl/6NCrl mice, these isoforms showed a distinct peak in the denaturation curves of the resulting amplicons, with no additional amplification products detected. (Figs. 20, 21, 22B). Gel electrophoresis unequivocally confirmed the specificity of the resulting amplicons, which were 119 bp (M variant), 95 bp (cChAT variant), and 125 bp (pChAT variant) in size

(Figs. 20, 21, 22C). The presence of a specific amplification product corresponding to GAPDH, which was used for normalization of the results, was confirmed.

In the PCR analysis of the M isoform of ChAT mRNA, a single amplification curve was observed across all examined GIT sections. Melting curve analysis revealed a single peak at 86 °C, and electrophoretic analysis confirmed the presence of the expected 119 bp product, verifying the specificity of the amplification (Fig. 20).

PCR analysis of the cChAT isoform in all examined GIT sections showed a single amplification curve. Melting curve analysis revealed a single peak at 81 °C, and electrophoretic analysis confirmed the presence of the expected 95 bp product, demonstrating the expression of this ChAT isoform throughout the digestive tract of the examined mice (Fig. 21).

Real-time PCR analysis of the pChAT isoform revealed a single amplification curve across all examined gastrointestinal tract samples. A single melting peak at 82 °C was observed, and agarose gel electrophoresis confirmed the expected 125 bp product, indicating the expression of the peripheral ChAT isoform in the mouse GIT (Fig. 22).

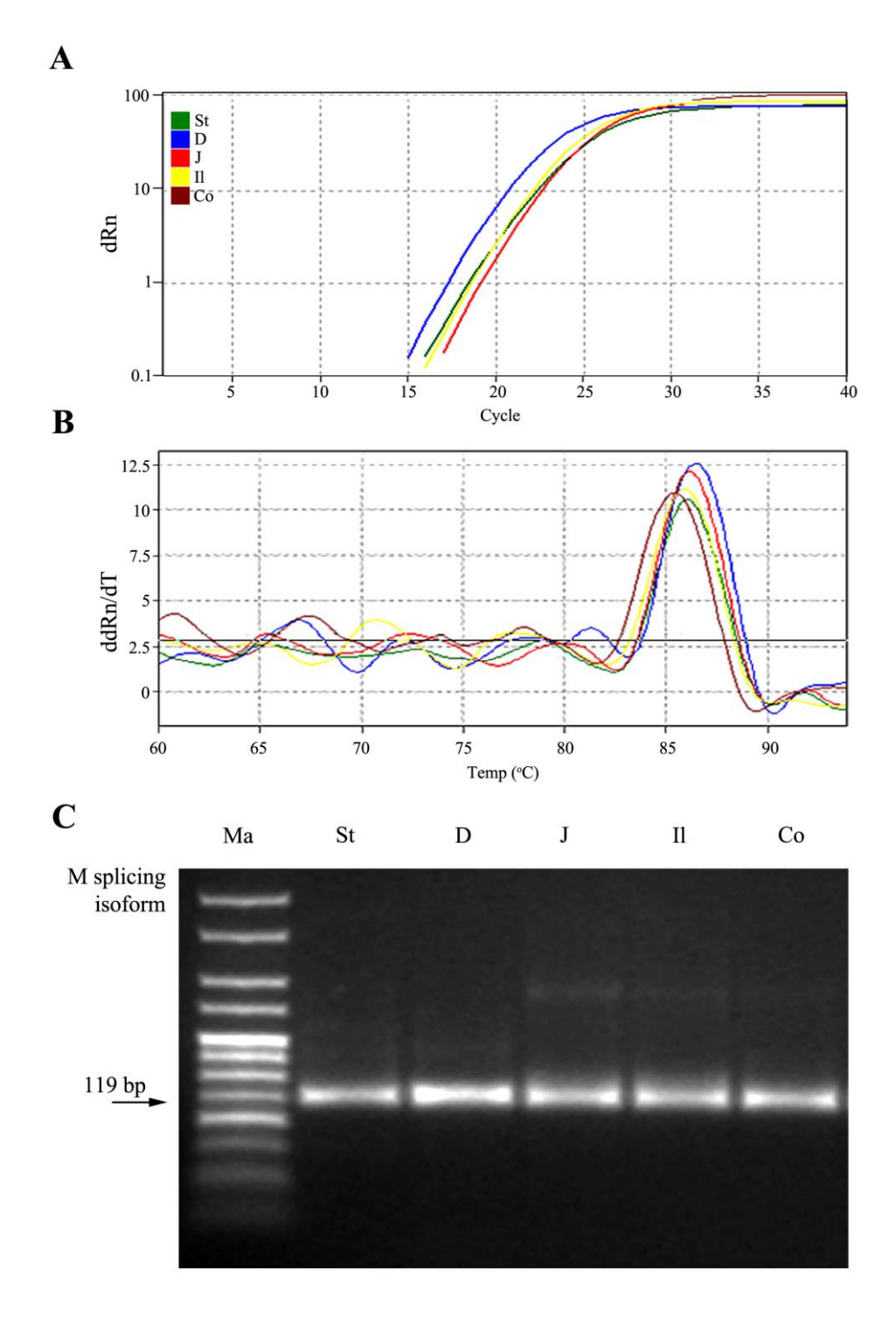


**Figure 20.** Representative qPCR using cDNA from the stomach, duodenum, jejunum, ileum, and colon of C57BL/6NCrl mice. (A) qPCR amplification; (B) melting curves of the specific products; (C) the resulting 119 bp product corresponds to the M isoform expressed in all regions examined.

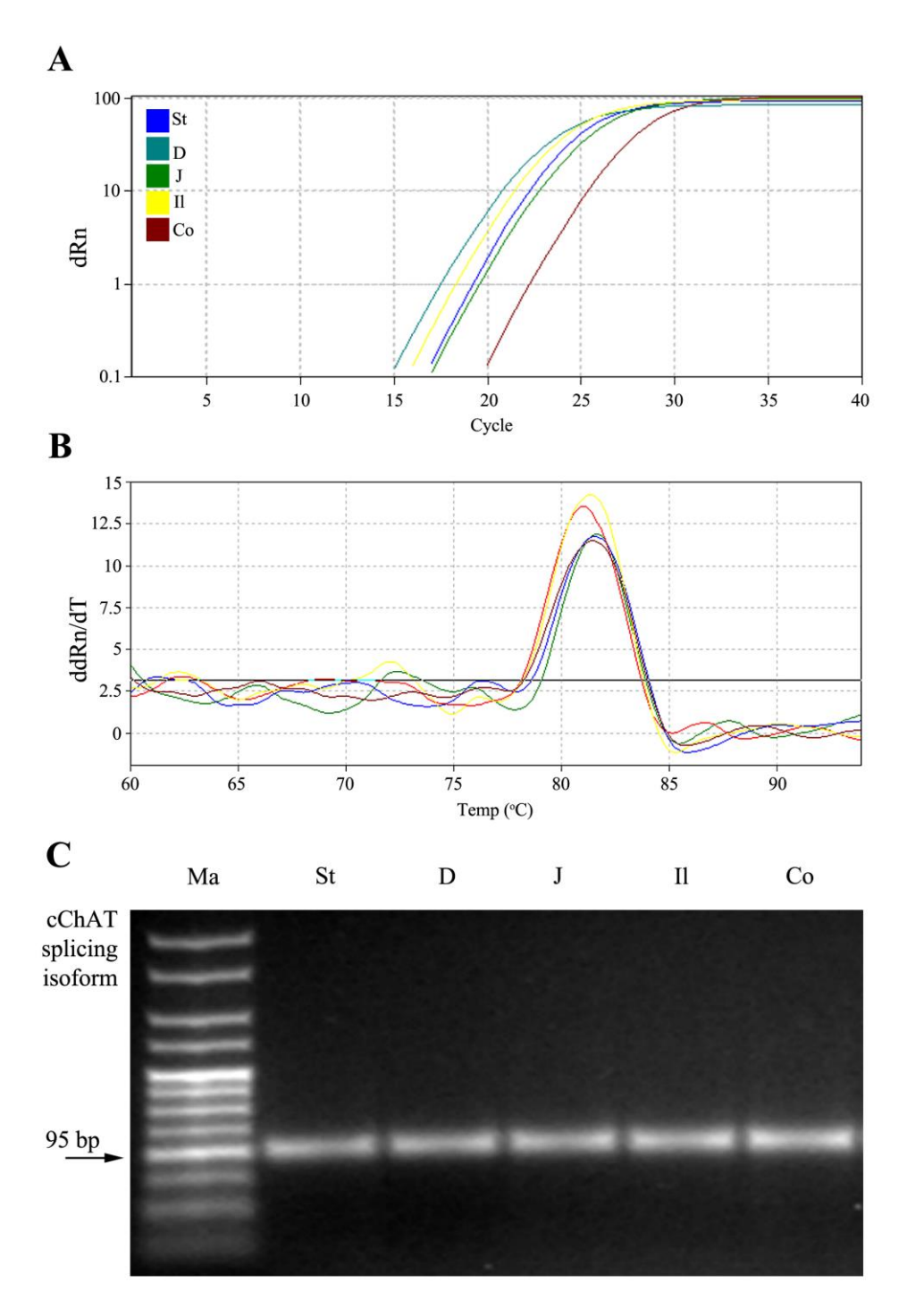


**Figure 21.** Representative qPCR using cDNA from the stomach, duodenum, jejunum, ileum, and colon of C57BL/6NCrl mice. (A) qPCR amplification; (B) melting curves of the specific products; (C) the resulting 95 bp product corresponds to the cChAT isoform expressed in all regions examined.

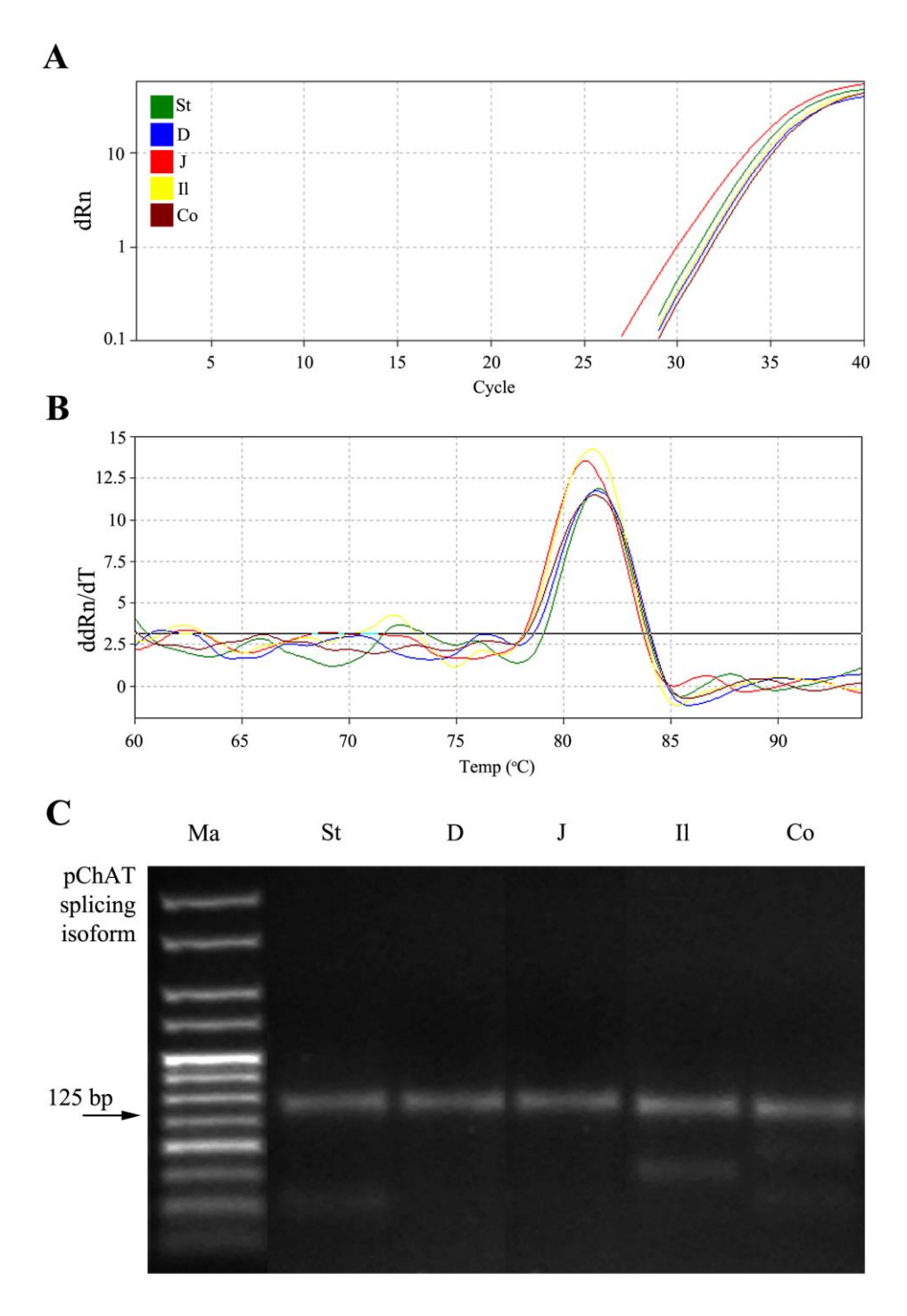


**Figure 22.** Representative qPCR using cDNA from the stomach, duodenum, jejunum, ileum, and colon of C57BL/6NCrl mice. (A) qPCR amplification; (B) melting curves of the specific products; (C) the resulting 125 bp product corresponds to the pChAT isoform expressed in all regions examined.

Expression analysis of the R3 isoform revealed a single amplification curve and a single melting peak in all examined GIT sections. However, the melting peak obtained using cDNA from different regions did not correspond to that observed with the *de novo* – designed synthetic template (gBlock-1). As shown in Fig. 23B, the melting temperature of the R3 variant analyzed with gBlock-1 (86 °C) differed by more than 10 °C from that obtained with

cDNA derived from the stomach, duodenum, jejunum, ileum, and colon (74 °C). Gel electrophoresis revealed products of identical length in all tested samples, which were shorter than the expected amplicon (Fig. 23B). The observed nonspecific amplification is likely due to primer dimer formation in the absence of template and at high primer concentrations. The absence of specific amplification products indicates that the R3 isoform is not expressed in the GIT of the examined mice, possibly due to inactivity of the corresponding promoter.

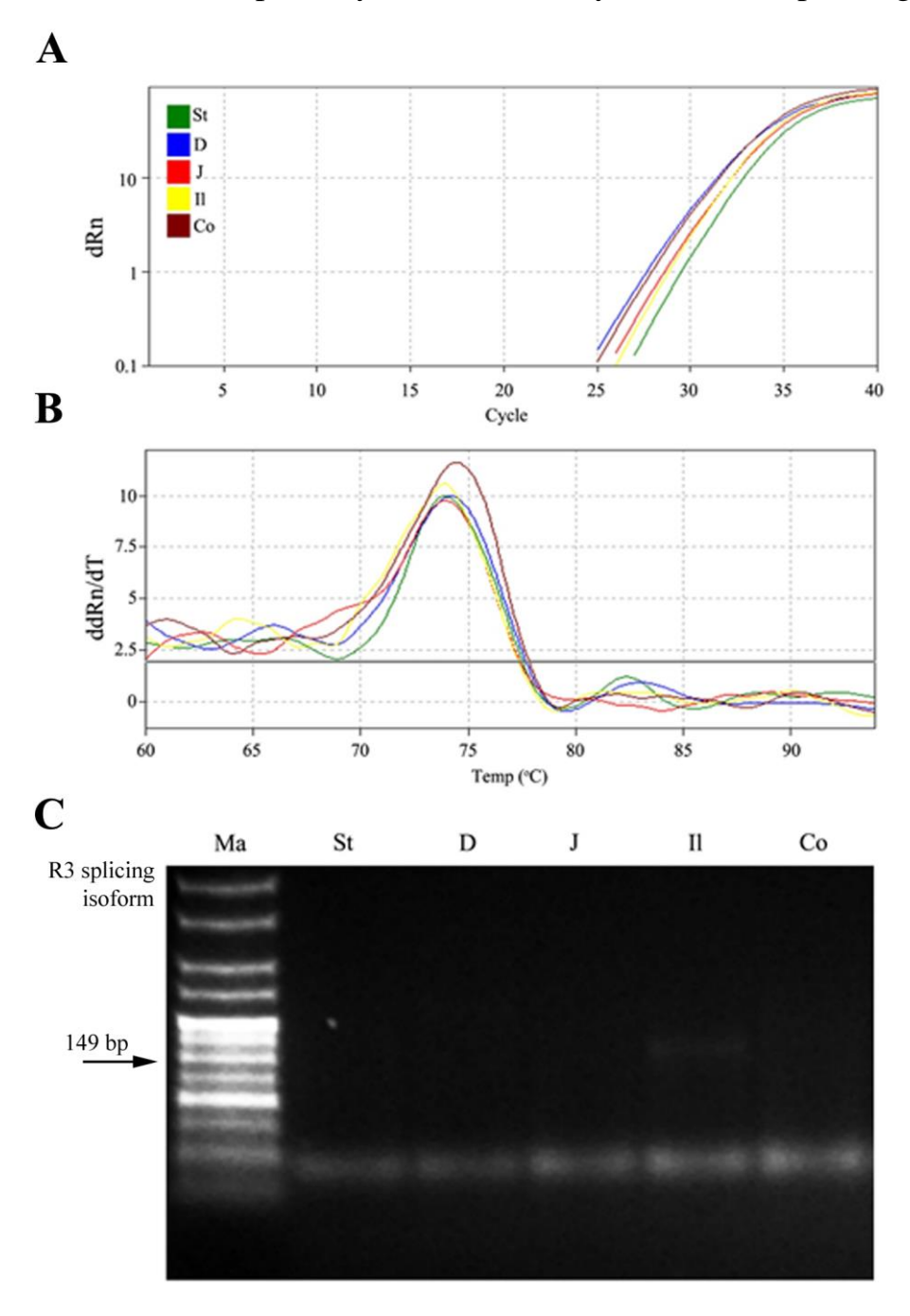


**Figure 23.** Representative qPCR using cDNA from the stomach, duodenum, jejunum, ileum, and colon of C57BL/6NCrl mice. (A) qPCR amplification; (B) melting curves of the obtained non-specific products; (C) the resulting product is approximately 50 bp in size, which does not correspond to the R3 isoform.

Expression analysis of the N1 isoform showed no amplification in the stomach and jejunum, while nonspecific products were detected in the remaining examined sections. Gel electrophoresis revealed bands larger than 300 bp (Fig. 24). The absence of the expected 170 bp amplicon suggests that this isoform may not be expressed in the GIT of adult mice.

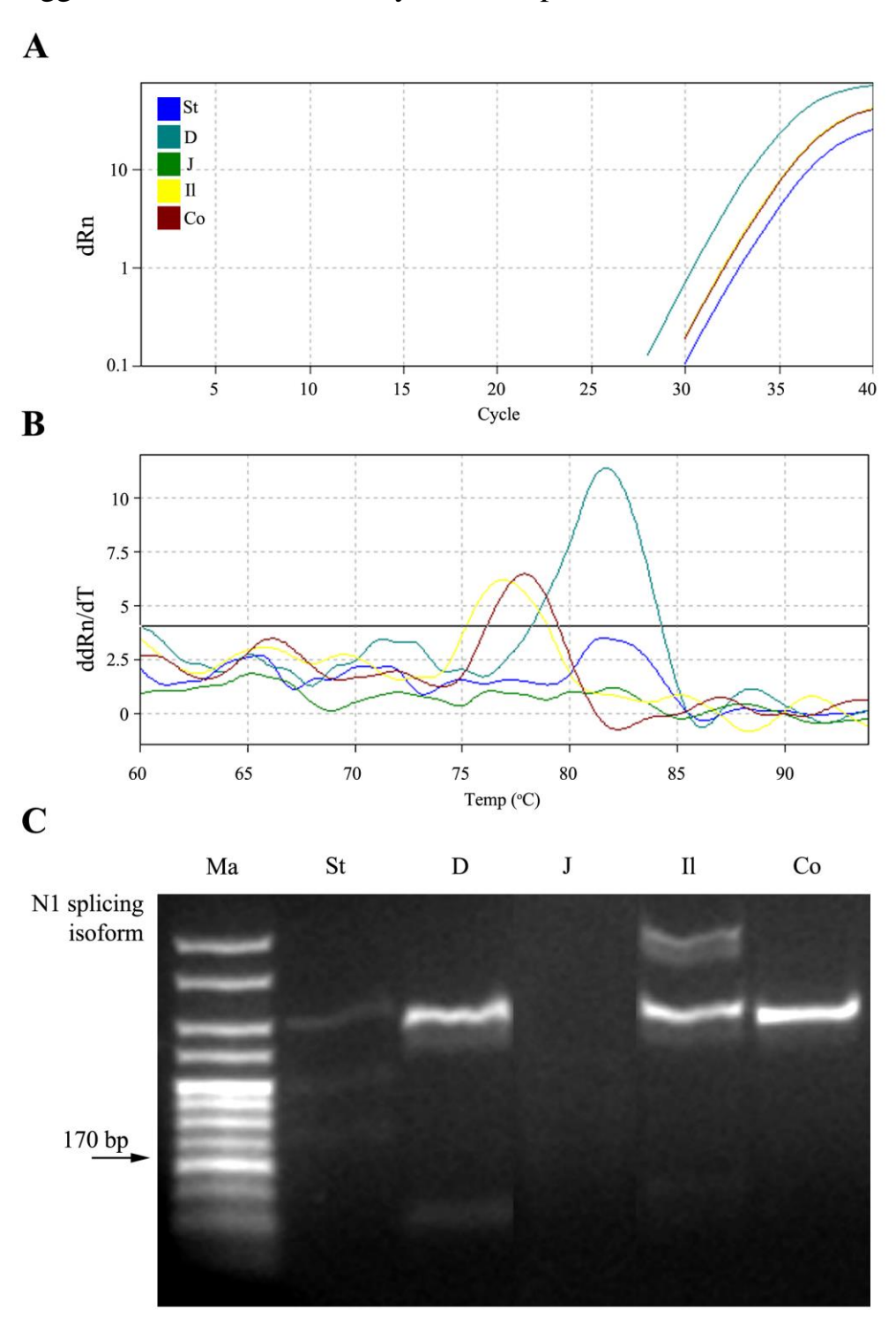


**Figure 24.** Representative qPCR using cDNA from the stomach, duodenum, jejunum, ileum, and colon of C57BL/6NCrl mice. (A) qPCR amplification; (B) melting curves of the obtained non-specific products; (C) the resulting products are larger than 300 bp, which do not correspond to the expected amplicon.

Expression analysis of the N2 isoform revealed nonspecific peaks in the melting curves and amplicons of lengths differing from the expected 112 bp. Primer dimers and additional nonspecific products were detected in almost all samples. These results likely indicate extremely low or absent expression of the N2 isoform in the GIT of the examined mice.

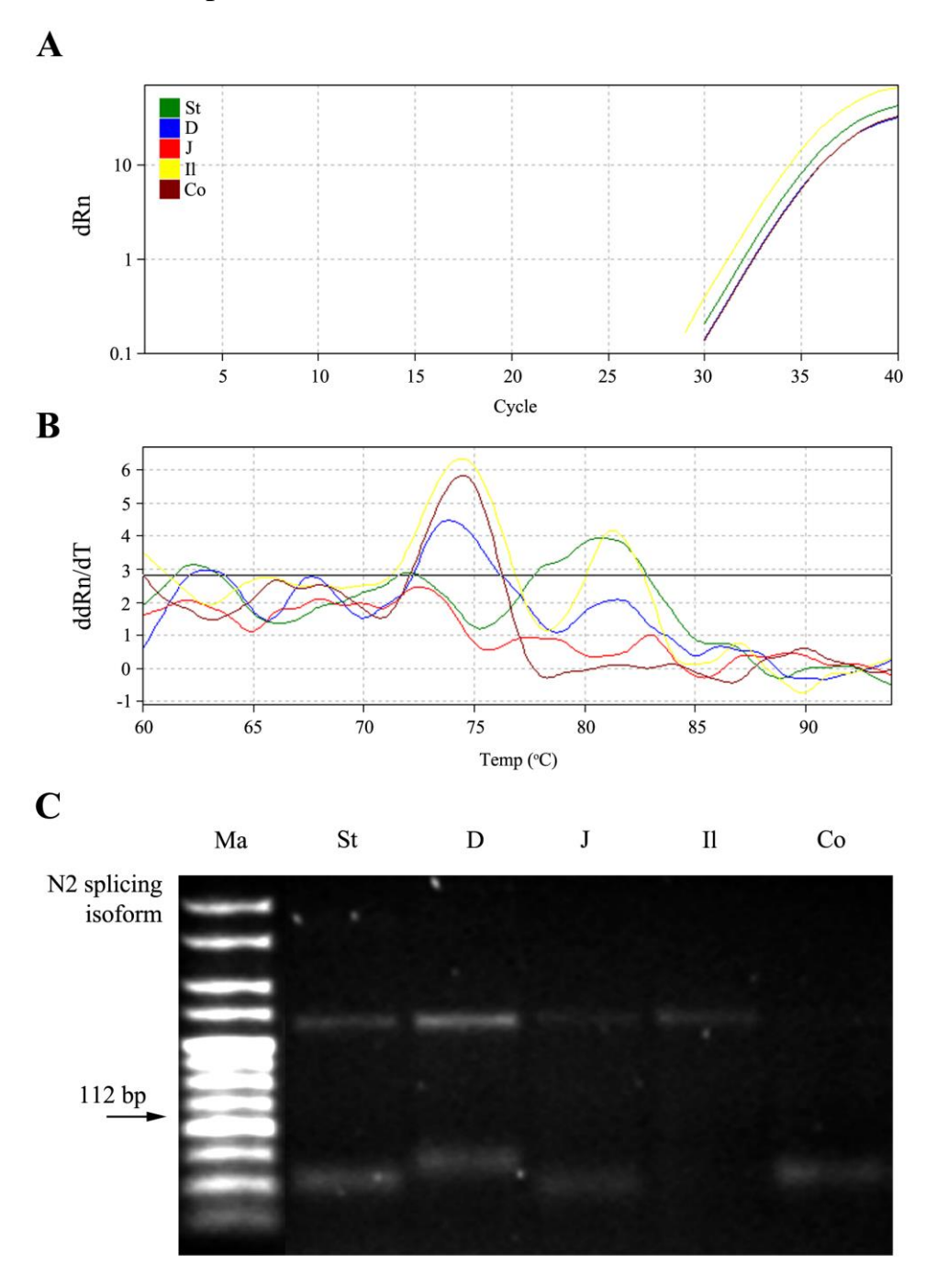


**Figure 25.** Representative qPCR using cDNA from the stomach, duodenum, jejunum, ileum, and colon of C57BL/6NCrl mice. (A) qPCR amplification; (B) non-specific melting peaks; (C) long-chain amplification products of a different size than expected, suggesting the presence of non-specific amplification and primer dimers.

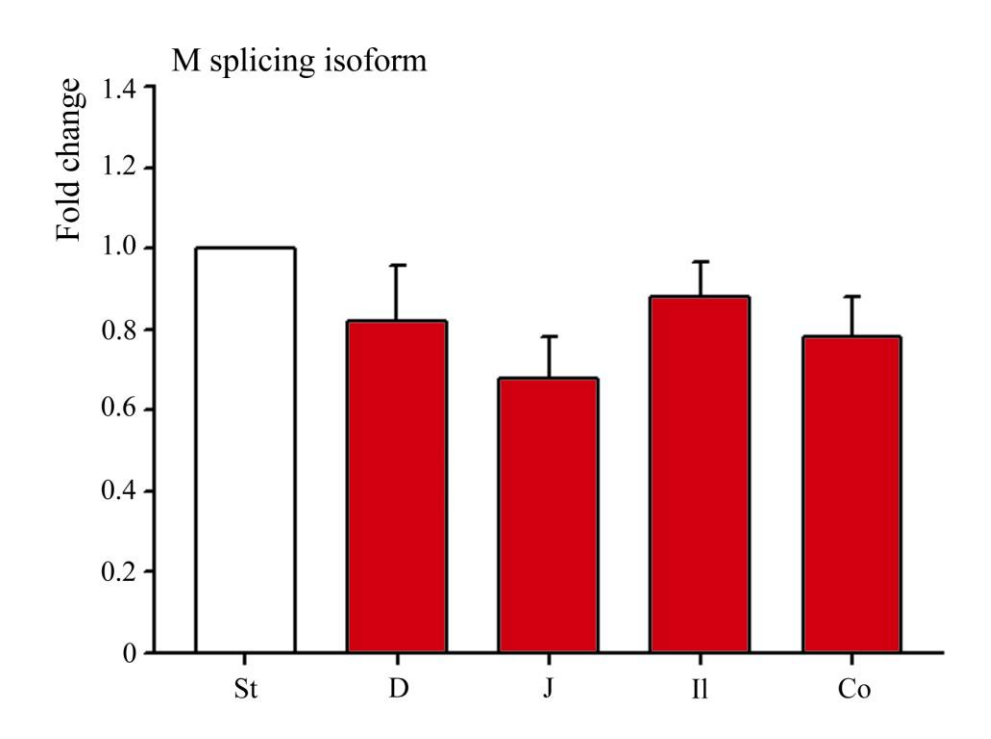
## 3.4. Relative quantitative PCR analysis of ChAT isoforms expression across different regions of the gastrointestinal tract in C57Bl/6NCrl mice

For the relative quantification of ChAT isoform expression in the GIT of C57Bl/6NCrl mice, analysis was performed using the modified  $\Delta\Delta$ Ct method according to Pfaffl. This approach accounts for the actual PCR efficiency of each specific isoform, as well as that of the reference gene (GAPDH). The relative abundance of each isoform was calculated as the ratio of the expression level of the target gene to that of GAPDH, relative to the corresponding control. The final expression levels were calculated using the following formula:

Ratio = 
$$\frac{\left(E_{target}\right)^{\Delta Ct_{target(control-sample)}}}{\left(E_{ref}\right)^{\Delta Ct_{ref(control-sample)}}}$$

Quantitative PCR was performed in three technical replicates for each organ (stomach, duodenum, jejunum, ileum, and colon). For each amplification product, Ct values were averaged to calculate  $\Delta$ Ct, defined as the difference between the average Ct value of the splicing isoform and the corresponding average Ct value of GAPDH for each tissue sample. The stomach was used as the reference tissue for calculating relative expression (fold change). E<sub>target</sub> and E<sub>ref</sub> represent the PCR efficiencies for the specific isoforms and GAPDH, respectively. The efficiency of each PCR reaction was determined in advance by generating standard curves (Figs. 19A-F).

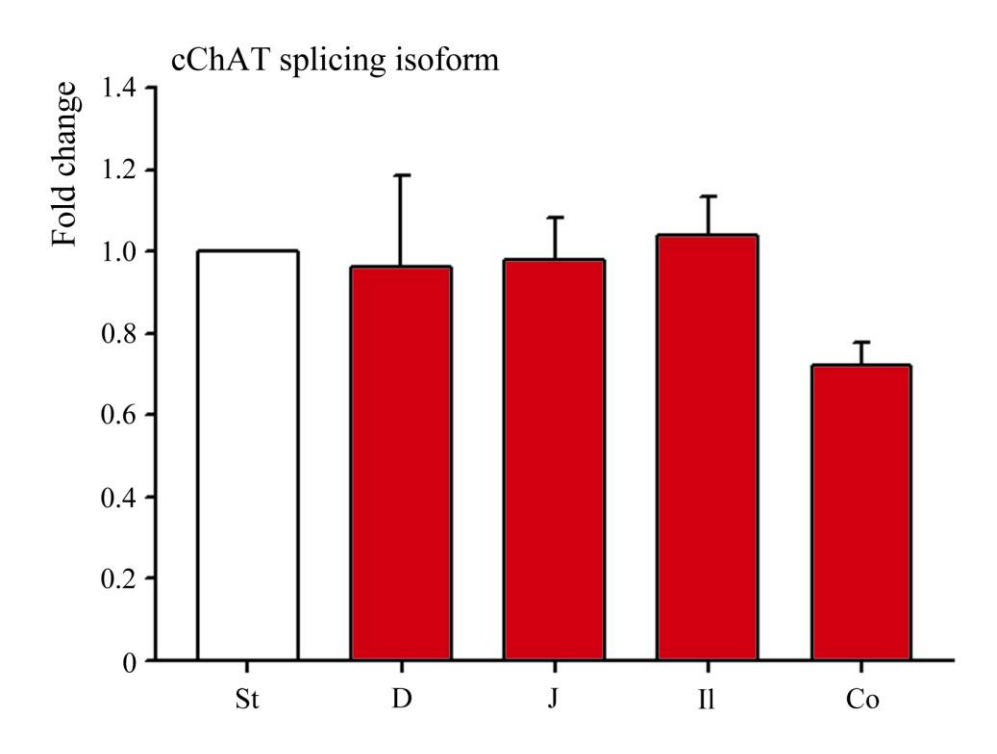
The relative expression of the M, cChAT, and pChAT splicing isoforms was calculated relative to the stomach, which was used as the reference organ (expression = 1.0). The M splicing isoform showed relatively stable expression along the GIT. In the duodenum, expression was  $80\% \pm 0.14$  relative to the stomach; in the jejunum,  $68\% \pm 0.10$ ; and in the ileum and colon,  $88\% \pm 0.09$  and  $78\% \pm 0.10$ , respectively. The greatest variability in expression was observed in the duodenum (Fig. 26).



Organs	Animals, n	Average	Standard deviation	SEM
St	5	1,000	0,000	0,000
D	5	0,820	0,311	0,139
J	5	0,680	0,228	0,102
I1	5	0,880	0,192	0,086
Co	5	0,780	0,228	0,102

Figure 26. Changes in the expression of the M splicing isoform relative to GAPDH in consecutive sections of the gastrointestinal tract (St – stomach, D – duodenum, J – jejunum, Il – ileum, Co – colon). Results are presented as relative changes (fold change) with standard deviations and standard error of the mean (SEM) included.

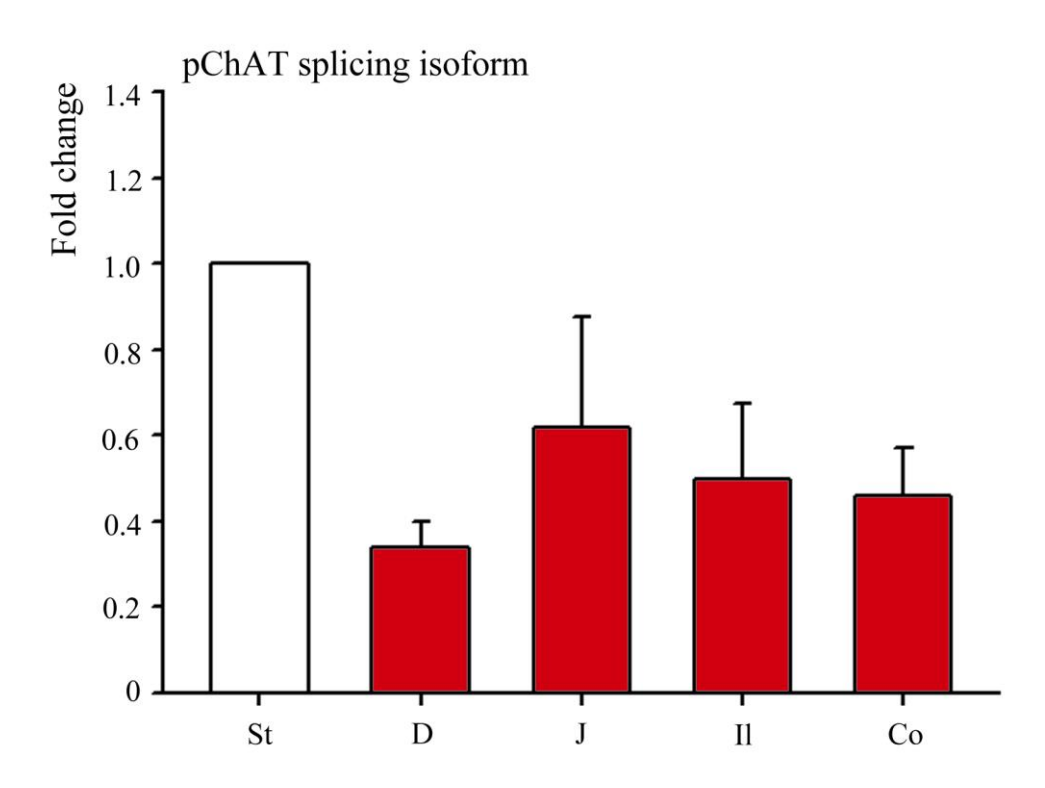
Analysis of the cChAT revealed relatively stable expression levels, comparable to those observed in the stomach. Expression was  $96\% \pm 0.18$  in the duodenum,  $98\% \pm 0.09$  in the jejunum, and slightly increased to  $104\% \pm 0.07$  in the ileum. In the colon, a trend toward decreased expression was observed, with values of  $72\% \pm 0.04$  (Fig. 27).



Organs	Animals, n	Average	Standard deviation	SEM
St	5	1,000	0,000	0,000
D	5	0,960	0,340	0,182
J	5	0,980	0,220	0,098
I1	5	1,040	0,160	0,072
Co	5	0,720	0,180	0,040

**Figure 27.** Changes in the expression of the cChAT splicing isoform relative to GAPDH in consecutive sections of the gastrointestinal tract (St – Stomach, D – Stomach

Statistical analysis of pChAT expression revealed significant differences compared with the M and cChAT splicing isoforms. Expression in the duodenum was significantly lower than the reference ( $34\% \pm 0.06$ ), whereas a significant increase was observed in the jejunum ( $62\% \pm 0.27$ ). Expression levels in the ileum ( $50\% \pm 0.13$ ) and colon ( $46\% \pm 0.18$ ) were similar, with no clear trend (Fig. 28).



Organs	Animals, n	Average	Standard deviation	SEM
St	5	1,000	1,000	1,000
D	5	0,340	0,160	0,062
J	5	0,620	0,600	0,268
I1	5	0,500	0,300	0,184
Co	5	0,460	0,240	0,107

**Figure 28.** Changes in the expression of the pChAT splicing isoform relative to GAPDH in consecutive sections of the gastrointestinal tract (St – stomach, D – duodenum, J – jejunum, Il – ileum, Co – colon). Results are presented as relative changes (fold change) with standard deviations and standard error of the mean (SEM) included.

Comparative analysis of the three ChAT splicing isoforms across the examined gastrointestinal regions revealed no statistically significant differences (ANOVA followed by Tukey's post hoc test). In the duodenum, relative expression levels were 82% for the M isoform, 96% for cChAT, and 34% for pChAT, with all values determined relative to the stomach which was used as a control (Fig. 29A).

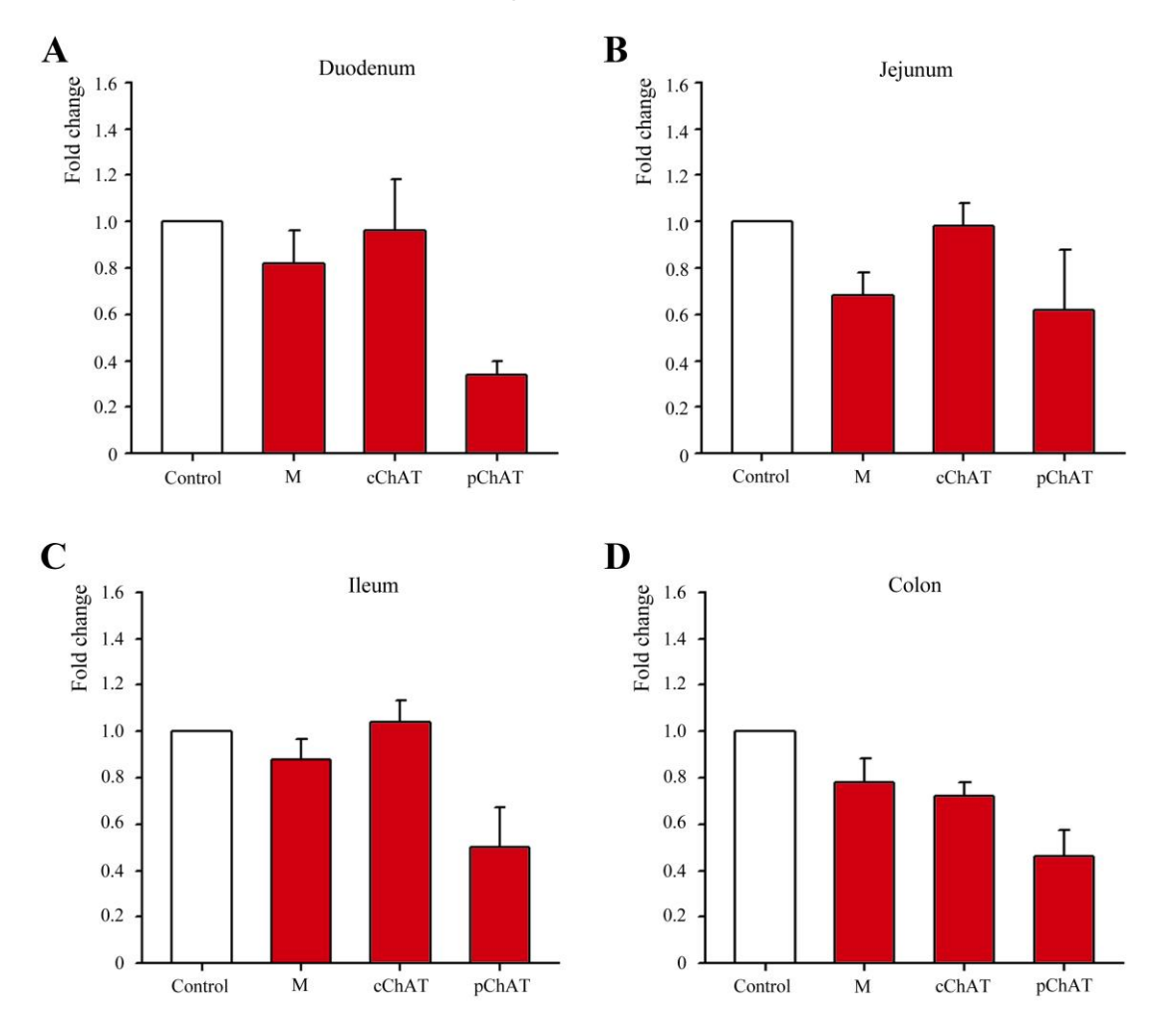


**Figure 29.** Changes in the expression of the M, cChAT, and pChAT splicing isoforms relative to GAPDH in the duodenum (A), jejunum (B), ileum (C), and colon (D). Results are presented as relative changes (fold change) with standard error of the mean (SEM) included. The stomach was used again as the reference organ.

Tracking of isoform expression in the jejunum revealed relative expression levels of 68% for the M isoform, 98% for cChAT, and 62% for pChAT compared to the stomach. Despite these apparent differences, statistical analysis showed no significant variation among the isoforms (ANOVA, Tukey's test) (Fig. 29B). In the ileum, expression levels were 88% for the M isoform, 104% for cChAT, and 50% for pChAT relative to the stomach (Fig. 29C). In the colon, expression reached 78% for the M isoform, 72% for cChAT, and 46% for pChAT (Fig. 29D). Similarly, no statistically significant differences between the isoforms were detected (ANOVA, Tukey's test).

#### **IV. Discussion**

### 1. Histological features of the digestive tract wall in C57Bl/6NCrl mice

The wall of the mouse digestive tract follows the general structural plan characteristic of tubular organs. This plan comprises four principal layers: an inner mucosal layer (tunica mucosa) with its own muscular lamina (lamina muscularis mucosae); a thin submucosal connective tissue layer (tela submucosa); a muscular layer consisting of an inner circular (stratum circulare) and an outer longitudinal (stratum longitudinale) layer; and an outer connective tissue layer, the tunica adventitia or tunica serosa. The mouse stomach is divided into two functionally and morphologically distinct regions: the forestomach and the glandular stomach (stomach proper). The forestomach represents the nonglandular compartment lined with stratified squamous epithelium, whereas the glandular stomach secretes gastric enzymes and acid. The small intestine consists of three segments, each with specific functional characteristics. The first segment, the duodenum, surrounds the pancreas and, at the level of the umbilicus, forms a U-shaped loop that continues into the jejunum. A distinctive feature of the mouse duodenum is the presence of submucosal Brunner's glands, which are limited to the first 2 mm of its length. The jejunum constitutes the major portion of the small intestine, followed by the short ileum, which represents its terminal segment. The colon begins distally at the ileocecal valve. In rodents, the cecum, which represents the initial part of the large intestine, is highly developed and occupies a substantial portion of the abdominal cavity, with its size and position varying according to the mode of feeding. Rodents lack an appendix. The colon is subdivided into proximal, middle, and distal segments, and terminates with a short rectum and the anus, which are characteristic features in mice.

The method of choice for a detailed study of the histological structure of the intestinal tract is the Swiss roll technique introduced by Reilly and Kirsner, which enables continuous visualization of relatively long sections of the intestine. Moolenbeek and Ruitenberg further recommended its use for examining the histological structure of the small intestine in rodents. Julie Le Naour et al. described a modified protocol based on the original Swiss roll technique to improve visualization of CD3-positive lymphoid structures in the colon of C57Bl/6J mice. They emphasized the advantages of this approach, particularly when fresh tissue is used, as it allows precise mapping of cell populations along the entire length of the colon.

In the present study, the Swiss roll technique was applied to investigate the histological features of the digestive tract wall in C57Bl/6NCrl mice. The analysis began with the forestomach, which displayed a stratified squamous nonkeratinized epithelium and a well-developed muscular layer (Fig. 8A). The stomach proper showed a glandular epithelium containing the full complement of cells that constitute the cardiac, fundic, and pyloric glands (Fig. 8B). The mucosa of the small intestine is distinguished by tall, well-developed intestinal villi, composed of absorptive enterocytes, goblet cells, and enteroendocrine cells (Fig. 8C –

E). The epithelium also contributes to local immune defense through the gut-associated lymphoid tissue (GALT), which plays a central role in the mucosal immune response. Deep within the lamina propria of the mucosa lie the intestinal glands, whose cellular composition includes columnar striated and nonstriated enterocytes, goblet cells, Paneth cells, and enteroendocrine cells. Beneath the mucosa, the thin submucosa contains Brunner glands only at the proximal duodenum, with their ducts traversing the layer and opening at the base of the crypts of Lieberkühn. In the large intestine, the predominant cell type – particularly within the intestinal glands – is the goblet cell, whose numbers gradually decline distally (Fig. 8F). A distinctive feature of the mouse colonic epithelium is the absence of Paneth cells, which contributes to the specificity of local immune defense. Another characteristic of the colonic mucosa is the presence of undulating folds that gradually decrease in size toward the distal colon.

The ENS forms an essential structural and functional component throughout the digestive tract. The plexus myentericus (Auerbach), located between the inner circular and outer longitudinal layers of the muscularis externa, was clearly visualized in our histological preparations (Fig. 8B-F). The myenteric ganglia forming the plexus myentericus vary in size, shape, and orientation across different compartments of the GIT. In the duodenum and jejunum, ganglia tend to be larger and more organized (Fig. 8C, D), whereas in the ileum they appear smaller and less frequent (Fig. 8E). Along the colon, myenteric ganglia reach their greatest size (Fig. 8F, Fig. 9A). In this region, they typically exhibit an oval to markedly elongated shape and are oriented parallel to the intestinal wall, consistent with previous reports. Using immunohistochemistry and cuprolinic blue staining, Karaosmanoglu et al. compared the density of myenteric neurons in the duodenum, jejunum-ileum, and colon. They reported a higher number of neurons in the duodenum and colon compared with the jejunumileum. Application of stretch resulted in a gradual decrease in neuron number. Regarding the area occupied by myenteric ganglia, the authors observed a larger area in the duodenumjejunum compared with the duodenum, which correlates with their length. The ganglion area was unaffected by stretching of the intestinal wall. According to the study, the myenteric ganglia occupy the largest area along the intestinal tract in the colon. Using immunohistochemistry and electrical stimulation, Zhiling et al. measured higher enteric neuron activity in the proximal colon compared with the distal colon in mice. Their findings indicate that enteric neural circuits vary across different regions of the intestinal tract. The authors reported more complex circuits in the proximal colon, associated with more diverse motor patterns and finer control by the ENS. Using modern genetic techniques and RNA sequencing, Nestor-Kalinoski et al. compared the size of individual myenteric ganglia and the number of neurons per ganglion along the mouse colon. Their study revealed a decrease in both the number of ganglia and the number of neurons per mm<sup>2</sup> along the colon. A

comparison with the human colon showed that mice have a significantly higher neuronal density per mm² than humans. Equivalent neuronal densities were observed between the proximal mouse colon and the human ascending colon, as well as between the distal mouse colon and distal human colon. A separate morphometric study in humans similarly demonstrated regional differences in the number of neurons in myenteric ganglia along the GIT. The authors observed a trend of decreasing neuronal density and ganglion size in the distal direction. In the rectum, similar to the stomach, they reported a slightly higher average number of neurons per cm² compared with the mesenteric small intestine and colon. The authors associate this characteristic of the rectum with the motor mechanisms underlying peristalsis and propulsion.

In the prepared histological sections, the plexus submucosus is located within the delicate layer of the mouse intestinal tract between the mucosa and the muscular coat (Fig. 8C-F). The plexus contains smaller ganglia scattered among the connective tissue fibers of the submucosa, with ganglion size correlating with the number of neurons (Fig. 9B).

The organization of the ENS reflects its diverse embryonic origins and the regionspecific patterns of migration, proliferation, and differentiation of its components along the GIT. Enteric neurons and glial cells arise from the vagal and sacral regions of the neural crest. The vagal neural crest, located at somites 1-7, supplies the majority of precursor cells for the ENS. These cells migrate in a rostro-caudal direction, colonizing the entire GIT between the 4th and 10th gestational weeks. In the distal segments of the intestine, ENS components originate from the sacral neural crest (located caudal to somite 28), which migrates later in a caudo-rostral direction. Recent studies have highlighted additional aspects of ENS organization, including the presence of peripheral bands oriented specifically along the gastrointestinal tract. Using immunohistochemistry, Hamnett et al. demonstrated that myenteric ganglia in mouse models are organized in stripe-like patterns with a circular orientation relative to the longitudinal axis of the intestine. This organization is maintained along the entire length of the intestinal tract. In contrast, the submucosal plexus of the small intestine does not exhibit such a striated arrangement, and its location does not correlate with that of the intraepithelial glands. In the proximal colon, the authors observed submucosal ganglia arranged in diagonal stripes, oriented parallel to the mucosal folds and positioned opposite the mesenteric border. This structural organization was not observed in the distal colon. These findings revise previous understandings of ENS morphology and provide opportunities for further studies on the pathophysiology of gastrointestinal motility.

## 2. Functional organization of the ENS

The enteric plexuses comprise a network of interconnected neurons, their processes, and complex reflex arcs that integrate information about the state of the digestive system and regulate local physiological processes. This complex neural apparatus functions relatively

independently of the central nervous system. Consequently, the ENS is often referred to as the "second brain" due to its high neuronal density and its autonomous control of bowel motility, intestinal secretion, and local blood flow. The ENS also governs mucosal transport as well as endocrine and immune functions of the gastrointestinal tract. Understanding the morphological features of the ENS and its interactions with the gut microbiome is crucial for elucidating the etiology of numerous gastrointestinal and systemic disorders. Structural and functional alterations of the ENS underlie functional gastrointestinal disorders such as achalasia, gastroparesis, intestinal obstruction, Crohn's disease, and Hirschsprung's disease. The role of the ENS in colonic malignancies has also been investigated. Moreover, an increasing number of studies link disruptions in the gut-microbiome-brain axis to the development of neurodegenerative diseases, including Alzheimer's disease, Parkinson's disease, and multiple sclerosis.

According to the literature, the ENS comprises approximately 20 distinct neuronal types, classified on morphological characteristics (Dogiel and Stach electrophysiological properties (S and AH types), neurotransmitter profile, and functional roles in intestinal regulation. One major functional class, the motoneurons, innervates the smooth muscle of the GIT, blood vessel walls, enteroendocrine cells, and glandular structures, playing a central role in controlling intestinal motility, secretion, and local blood flow. Neurons that respond to chemical and mechanical stimuli within the intestinal wall are classified as intrinsic primary afferent neurons (IPANs). These neurons constitute the first step in the ENS local reflex arcs and are crucial for sensing changes in the chemical environment and mechanical tension of the mucosa and muscular layers of the GIT. Von Haller was the first to demonstrate that isolated intestines can retain their ability to respond to sensory stimuli despite being disconnected from the brain and spinal cord. Definitive evidence for the sensory function of enteric neurons was not provided until the mid-1990s by Furness. Studies by Furness and Kunze showed that enteric neurons with Dogiel type II morphology are responsible for detecting both chemical and mechanical stimuli. Neurons with Dogiel type I morphology have also been suggested to possess mechanosensory functions, but unlike type II neurons, their projections do not reach the mucosa.

The GIT utilizes multiple neurotransmitters and biologically active molecules, which can be co-stored and released in response to specific stimuli. These mediators play a crucial role in modulating peristalsis, secretory activity, and local immune responses. All neuroactive substances acting within the ENS contribute to the maintenance of intestinal homeostasis. Substance P is directly involved in pain signaling, whereas vasoactive intestinal peptide (VIP) regulates the proliferation of goblet cells and stimulates mucin secretion from the intestinal mucosa. Additionally, VIP modulates immune cell functions within the ENS and participates in smooth muscle relaxation. Serotonin (5-HT) regulates the activity of multiple enteric

neurons, glial cells, and immune cells. ACh serves as the principal excitatory neurotransmitter in the ENS, controlling and regulating numerous physiological processes in the GIT. It is a major transmitter for preganglionic vagal and pelvic neurons and is widely utilized by enteric motoneurons, interneurons, certain secretomotor neurons, and IPANs. In addition to its neuronal function, ACh also acts as a signaling molecule in various non-neuronal cells, which express ACh and use it to regulate diverse cellular processes. Recent evidence suggests that neuronal ACh may also serve as a mediator in the development and proliferation of neoplastic formations, including human colorectal cancer. The primary enzyme responsible for ACh synthesis is ChAT. Investigating the different isoforms of the mRNA encoding this enzyme and their expression is essential for understanding the molecular mechanisms underlying a variety of diseases.

## 3. Genetic analysis of ChAT: molecular strategies for identifying and visualizing ChAT isoforms in the mice

The ChAT enzyme is encoded by a single gene in all animal species studied to date. In mice, the ChAT gene contains 17 exons, including three 5'-noncoding exons (R, N, and M) followed by 14 successive coding exons (Fig. 1A, B). The entire open reading frame of VAChT mRNA is located within the first intron of the ChAT gene locus, between the R and N noncoding exons. The third M noncoding exon is situated between the N and the first Nterminal coding ChAT exon (Fig. 1A). Multiple transcription initiation sites, likely corresponding to promoter regions, increase the likelihood that distinct ChAT mRNAs are expressed in different cholinergic neurons and non-neuronal cell types. Misawa et al. identified seven splicing isoforms of ChAT mRNA in the mouse: M, N1, N2, R1, R2, R3, and R4. All isoforms differ in their 5'-noncoding regions, encoding the same protein of 67 kDa, representing the cChAT. Among these transcripts, the M isoform is the most prevalent in the mouse spinal cord. In total, 21 transcripts were isolated in this study, 19 of which contained exon M. Of these 19 transcripts, four were M isoforms, while the remaining 15 included part of exon M, as seen in the N1, R3, and R4 isoforms. Using transfection analysis, Misawa et al. demonstrated the presence of a highly efficient promoter upstream of exon M, supporting the predominant role of the M isoform in ChAT expression in mice. Their study also added the R3 and R4 variants to the five previously described by Mineko Kengaku in the rat: R1, R2, N1, N2, and M. Genetic analysis of splicing isoforms in the rat by Kengaku et al. confirmed that the M isoform is the most prevalent among spinal cord transcripts. Of the 29 cDNA copies isolated from the spinal cord, six were M isoforms, four were R1, two were R2, one was N, and 16 were classified as either M or N1 isoforms.

Analysis of the human genome and the described splicing isoforms of ChAT indicate the presence of a distinct start codon at the beginning of the coding region of the gene. In rodents and pigs, this codon is the classical ATG, whereas in humans the corresponding site

contains the sequence ACG, which does not function as a translation initiation codon. All splicing isoforms identified in the human brain encode a protein with a molecular weight of 69 kDa. PCR analysis of ChAT mRNA in human brain and spinal cord by Misawa et al. revealed expression of an R isoform 277 bp in length, which corresponds to the R2 isoform described in rodents. The R3 and R4 isoforms were not detected in humans. Using an Nspecific primer pair, three amplification products were observed, corresponding to the N1 and N2 isoforms. The third, longer product contained identical 9 bp repeated nucleotide sequences. Amplification with M isoform-specific primers produced a single 458 bp product in both brain and spinal cord. Within this M isoform, two ATG codons flank the nonfunctional ACG codon, whereas in the R, N1, and N2 isoforms only a single ATG codon is located downstream of the ACG. Subsequent in vitro translation analysis revealed two translational products of the M isoform: one with a molecular mass of 69 kDa, analogous to all other splicing isoforms, and a second with a mass of 82 kDa. Overall translational efficiency of the isoforms was low, with the M isoform showing particularly reduced efficiency. In conclusion, the authors demonstrated high expression of the M isoform in the human CNS, consistent with the expression profile observed in rodents. In contrast to the high transcriptional activity, translational efficiency in humans remains low. This discrepancy between the abundance of ChAT mRNA and the actual synthesis of the enzyme indicates the presence of human-specific posttranscriptional or translational regulatory mechanisms. The reduced translational efficiency of human ChAT mRNAs compared with rodents likely reflects an evolutionarily determined adaptation of the cholinergic system to distinct functional demands. Although the structure of the mouse ChAT gene and its regulatory elements has been extensively studied, knowledge of the expression patterns of alternative splicing isoforms of ChAT mRNA and the activity of different promoters along the gene remains incomplete and insufficiently explored. Only a subset of ChAT mRNA splicing isoforms has been demonstrated using methods such as in situ hybridization, reverse transcription PCR, and immunohistochemistry. Trifonov at al. analyzed the expression of N1, R1, R2, R3, and R4 isoforms in the mouse CNS by nonradioactive in situ hybridization. The study revealed region-specific expression patterns across cholinergic structures, including the basal forebrain complex, pontomesencephalic tegmentum, striatum, and motor and autonomic nuclei of the brainstem and spinal cord. The highest expression of R1 and R2 was observed in the basal forebrain complex and brainstem nuclei. In motor and autonomic nuclei of the brainstem, moderate to high levels of R3, R4, and N1 expression were detected, whereas forebrain cholinergic structures showed only weak expression. No expression of N1 or R1-R4 was detected in neurons of the cerebral cortex, hippocampus, or medial habenular nucleus, indicating predominance of the M isoform in these areas. Semi-quantitative RT-PCR confirmed this region-specific profile. In the striatum, high expression of R1, R2, and R4 was

found, with lower expression of R3 and minimal expression of N1. In the medulla oblongata, by contrast, N1, R3, and R4 were expressed at nearly equal levels, accompanied by higher expression of R1 and R2. Notably, no amplification product corresponding to the N2 isoform was detected, suggesting absent or very low expression of this isoform in the regions studied.

Available literature on the expression of ChAT splicing isoforms in the ENS is largely restricted to immunohistochemical visualization of pChAT in the enteric plexuses of mouse, guinea pig, rat, pig, monkey, and human. These morphological approaches provide valuable insights into the localization of cholinergic neurons but do not permit quantitative assessment of isoform expression. This limitation underscores the need to complement morphological data with molecular genetic methods, which enable quantitative and reproducible characterization of ChAT expression profiles in the ENS. For this study, isoform-specific forward and reverse primers targeting the R3, N1, N2, M, cChAT, and pChAT splicing isoforms of ChAT mRNA were designed using Primer-BLAST (Table 1). Primer design followed standard criteria for efficient PCR amplification, including a Tm of 60-65 °C and GC content of 40-60%, to ensure specificity and stable hybridization. Fluorescence-based PCR is the method of choice for quantifying low-abundance, alternatively spliced mRNA isoforms. Reliable quantification requires careful optimization of primer selection, reverse transcription, and amplification conditions. The establishment of absolute or relative standards is critical, which can be achieved using circular or linear plasmids carrying unique fragments of each isoform. An alternative strategy involves the use of synthetic doublestranded linear DNA fragments carrying the specific sequences of each ChAT splicing isoform, along with a reference fragment. These synthetic constructs serve as precise templates for establishing highly specific standards in absolute quantification assays. In this study, de novo synthesized double-stranded gBlock gene fragments (gBlock-1 and gBlock-2), together with the plasmid pGEM-N containing isoform-specific nucleotide sequences, were employed as templates for PCR amplification. Each template was used to validate the corresponding primer pairs designed for the detection of individual ChAT splicing isoforms. Because of the high sequence similarity among ChAT mRNA isoforms, establishing a specific and reproducible quantification method is technically demanding. This necessitates rigorous primer design targeting unique exon regions for each isoform, followed by verification of the amplified products through electrophoretic analysis. Quantitative PCR offers distinct advantages, including high sensitivity, specificity, and reproducibility, making it particularly suitable for assessing the expression of ChAT splicing isoforms. Three main strategies are available for their quantification: 1) use of isoform-specific primers targeting unique exons or nucleotide sequences; 2) use of primers designed across exon–exon junctions paired with a primer located in a common exon; 3) use of fluorescent probes hybridizing at exon—exon junctions in combination with common primers. The third approach, which relies

on common primers combined with isoform-specific boundary probes, is considered less reliable. The use of common primers in combination with unique boundary probes is considered an unreliable approach, because when one alternatively spliced isoform is expressed at low levels and another at high levels, co-amplification of the predominant transcript by the common primers may hinder the accurate and quantitatively reliable detection of the low-abundance isoform. When isoform-specific primers cannot be designed due to high sequence homology among ChAT splicing isoforms, primers targeting unique exon—exon junctions are recommended. This strategy is especially effective when expression levels differ substantially between isoforms, as it enhances amplification specificity and enables reliable discrimination of individual splicing isoforms.

Wong et al. developed a real-time PCR approach to quantify the expression of three splicing isoforms of  $GFR\alpha$ -2 –  $GFR\alpha$ -2a,  $GFR\alpha$ -2b, and  $GFR\alpha$ -2c – which differ in their 5′-noncoding regions.  $GFR\alpha$ -2 serves as a primary receptor for the neurotrophic factor neurturin (NTN), which is involved in the protection of dopaminergic neurons. Due to the high sequence similarity and absence of unique nucleotide regions among the isoforms, the authors designed primers spanning exon—exon junctions, paired with a primer in a common exon. This validated methodology was subsequently applied by Too et al. to quantitatively assess the expression of  $GFR\alpha$ -2 isoforms in mouse brain, small intestine, kidney, liver, and testis. The absence of unique exons in the N2 and pChAT isoforms examined in this study required the use of reverse primers crossing the exon—exon junctions, with five nucleotides complementary to the specific junction of each isoform. This approach has been proven effective for detecting alternative splicing isoforms with a high degree of homology, as it prevents nonspecific amplification even in the presence of a dominant major transcript.

Regarding the R isoforms, suitable primers for identifying the R2 were not developed during the experiment due to the lack of unique primer-binding regions in this splicing isoform. The primers for isoforms R1 and R4 were designed to hybridize at exon—exon junctions; however, similar to the R2 isoform, they exhibit high homology with isoforms R3, N1, and M. Testing of the designed primers for R1 and R4 with test templates produced amplification products corresponding to regions shared with the highly homologous isoforms. Of the five boundary nucleotides at the 5' end of the R1 isoform, only three were specific, which explains the nonspecific amplification obtained. For the R3, by contrast, a specific primer pair was successfully designed. When tested with the gBlock-1 template, an amplification product of the expected length of 149 bp was obtained. However, subsequent testing with tissue samples from the experimental animals revealed an amplification product of smaller size (~50 bp) and a lower melting temperature (Tm 72-73 °C) in all examined sections of the GIT. These results did not correspond to the data from the preliminary analysis with the control DNA template. The obtained products were primer dimers, and their

amplification resulted from the absence of a template with which the primers could hybridize. The lack of expression of the R isoforms in the ENS of adult mice, observed in our study, correlates with the absence of expression of these splicing isoforms in blood cells. Fujii and Ogawa reported that R splicing isoforms of ChAT mRNA are not expressed in two T cell lines, CEM and MOLT-3. In CEM cells, the predominant isoforms were N2 and M, with lower levels of N1, whereas MOLT-3 cells expressed only the N2 isoform. RT-PCR also confirmed the absence of VAChT mRNA in both cell lines. These findings support the notion that the regulatory mechanisms governing ChAT mRNA expression in T lymphocytes differ markedly from those in cholinergic neurons of the CNS. In contrast, in the spinal ganglia of 15-day-old Wistar rats, both VAChT mRNA and the corresponding protein were detected by RT-PCR and Western blot analysis. In a study on rats, Corsetti et al. investigated the expression of two major cholinergic markers, ChAT and VAChT, during spinal ganglion development. Expression was analyzed at embryonic day 18 and on postnatal days 2, 15, and 60. Using isoform-specific primers, the authors detected multiple ChAT splicing isoforms (R1, R2, N1, N2, and M) and VAChT isoforms (R1, R2, V1, and V2). Quantitative RT-PCR revealed a progressive decline in the expression of all examined isoforms throughout ontogenetic development. During the embryonic period, the highest expression levels were observed for the R1 and R2 isoforms, while the M isoform was detected exclusively at this stage. The N1 and N2 isoforms were present at all ages examined, although their expression declined significantly after birth. In contrast, Western blot analysis revealed increasing levels of ChAT and VAChT proteins with age. This discrepancy between mRNA isoform expression and protein abundance suggests posttranscriptional regulation of both cholinergic markers. The authors propose that the reduced levels of mRNA isoforms may serve as an adaptive mechanism to prevent excessive accumulation of the corresponding proteins, particularly in sensory neurons where Ach is not a primary neurotransmitter.

High levels of two ChAT mRNA transcripts, approximately 3.5 kb and 1.3 kb in length, were detected in rat testis. Northern blot analysis using testis RNA and sequenced cDNA fragments spanning the entire coding region revealed that both transcripts share identical 5' ends. However, the shorter transcript contains only the first 800 nucleotides of the coding sequence, making it incapable of encoding a functional ChAT protein. Again, in the rat testis, Lönnerberg at al. reported expression of the short-chain variant of the enzyme, which lacks ChAT activity. These findings suggest that mammalian testes do not express a fully functional ChAT but instead produce truncated isoforms that likely serve testis-specific roles. Notably, an alternative ChAT mRNA isoform lacking the sequence corresponding to coding exons 6–9 was first described in rat. Yasunara demonstrated expression of the short isoform of ChAT in cholinergic neurons of the rat trigeminal ganglion and ciliary ganglion. In a related study, Tooyama analyzed cDNA from the striatum and pterygopalatine ganglion using

three primer pairs targeting the 5' end, middle region, and 3' end of the enzyme's cDNA. Electrophoretic analysis revealed a product of the expected length (1935 bp, corresponding to cChAT) in both tissues. In addition, a shorter product was detected in the pterygopalatine ganglion. Sequence analysis showed that this shorter isoform lacked 630 nucleotides from the central portion of the enzyme's cDNA, while the 5' and 3' flanking regions were identical to the full-length transcript. According to the genomic structure of rat ChAT, which consists of 15 exons, the newly identified isoform lacks exons 6–9. Because the number of omitted nucleotides is an exact multiple of three, the alternative splicing event preserves the open reading frame. The translation product of this splicing isoform has a molecular weight of 49 kDa and has been termed the peripheral type ChAT (pChAT) due to its detection in structures outside the CNS. The distinctive structure of the short-chain isoform, characterized by a splicing junction between exons 5 and 10, enabled Tooyama and Kimura to generate a rabbit antiserum against a recombinant 41-amino acid peptide spanning this exon-exon boundary. This antiserum was applied in Western blot and immunohistochemical assays, confirming that the pChAT was localized specifically to the neuronal cell bodies and processes in the ganglion pterygopalatinum. To assess its distribution in other peripheral tissues, the authors examined rat intestine using double labeling with the pChAT antiserum and NADPHdiaphorase histochemistry. The analysis revealed cholinergic neurons (brown) that were also positive for NADPH-diaphorase (blue) in the enteric plexuses of both duodenum and colon. Through fluorescence immunohistochemistry, Elnasharty and Shoeib identified pChATimmunoreactive neurons in the guinea pig ganglion trigeminale. Using dual immunolabeling, they demonstrated colocalization of the peripheral ChAT isoform with sensory markers CGRP and substance P, indicating a role of pChAT in pain signaling pathways. Prior to the discovery and visualization of pChAT by Tooyama and Kimura, the existence of distinct isoforms of the ChAT enzyme had not been recognized.

The ENS, as a major division of the peripheral nervous system, contains neurons and their processes that extensively express pChAT. In guinea pig experiments, Roberto Chiocchetti demonstrated strong pChAT immunoreactivity in IPANs located in the submucosal and myenteric plexuses. These neurons were calbindin-positive and exhibited only weak cChAT immunoreactivity. In contrast, calretinin-positive neurons, including motor neurons and interneurons within the myenteric plexus, showed strong cChAT immunopositivity. By distinguishing these neuronal subpopulations, Chiocchetti provided evidence that the two splicing isoforms of ChAT are functionally segregated, serving different classes of enteric neurons. Notably, neurons lacking detectable cChAT, the principal enzyme for ACh synthesis, appear to rely instead on the short-chain pChAT isoform.

Using the pChAT antiserum developed by Tooyama and Kimura, immunohistochemical tracing extended the findings from the ganglion pterygopalatinum to the entire GIT in rat and

guinea pig. Nakajima et al. were the first to demonstrate pChAT-positive neurons and processes in both the myenteric and submucosal plexuses from the esophagus to the rectum. Double staining in rat tissue revealed that nearly all pChAT-immunoreactive neurons also displayed acetylcholinesterase (AChE) activity but not NADPH-diaphorase reactivity. Morphologically, pChAT-positive neurons in the submucosal plexus showed Dogiel type I characteristics in the upper GIT and Dogiel type II features in the lower compartments. In guinea pig, some neurons exhibited dual positivity for pChAT and NADPH-diaphorase, while isolated AChE-positive but pChAT-negative neurons were also observed. Complementary PCR analysis using a primer pair producing a 124 bp amplicon confirmed the presence of the pChAT splicing isoform in the ganglion pterygopalatinum and in the duodenum.

Our genetic analysis confirmed the expression of the pChAT isoform throughout the GIT, consistent with previous reports. Alongside pChAT, the detection of M and cChAT isoforms demonstrates the coexistence of multiple transcriptional isoforms of ChAT in the ENS. The simultaneous expression of these three isoforms points to functional heterogeneity among cholinergic neurons and suggests that each may contribute differently to the regulation of motor and secretory functions. The confirmation of M isoform expression, known to predominate in rodent CNS, further supports the concept of structural and functional parallels between central and enteric cholinergic systems. The concurrent presence of pChAT and cChAT underscores the need to clarify their distinct regulatory roles under both physiological and pathological conditions.

In the present study, relative quantitative analysis by qPCR was employed to evaluate the expression of alternative splicing isoforms of the ChAT enzyme. This method enables comparison of target gene expression to that of a stably expressed internal reference gene, thereby accounting for potential variability in RNA quality, quantity, and reverse transcription efficiency. The most widely applied strategy for relative quantification is the  $\Delta\Delta$ Ct method (Livak and Schmittgen), which determines expression differences between tissues or experimental conditions by comparing the cycle threshold (Ct) values of target and reference genes. For reliable application of this method, PCR amplification efficiencies of both genes must be similar and close to 100%, with an acceptable deviation of no more than 5%. The basic steps of the  $\Delta\Delta$ Ct method are as follows:

- 1. Normalize the Ct values of the target gene to those of the reference gene (calculate  $\Delta$ Ct);
- 2. Compare  $\Delta$ Ct values with a control sample (calculate  $\Delta\Delta$ Ct);
- 3. Determine relative expression using the formula  $2^-\Delta\Delta Ct$ .

When amplification efficiencies of the target and reference genes deviate substantially from 100%, the alternative approach described by Pfaffl is applied. This model incorporates

the specific PCR efficiency of each gene, thereby providing a more accurate representation of relative expression levels.

In the present study, Pfaffl's formula was used, enabling reliable comparison of ChAT splicing isoforms across different compartments of the GIT. This strategy eliminates the need for absolute quantification and permits assessment of tissue-specific differences in isoform expression in relation to the functional characteristics of individual GIT regions. During the statistical analysis, three ChAT isoforms (M, cChAT, and pChAT) were successfully detected along the GIT of the mice examined in this study. Expression analysis showed that the M isoform was characterized by relatively constant levels across all examined segments, comparable to those observed in the control organ (stomach). The expression of cChAT was also similar to the control in the proximal segments of the small intestine (duodenum and jejunum), with a slight increase observed in the ileum, while a decrease in expression was detected in the colon. The most pronounced deviation in the expression profile was observed for pChAT: expression was markedly reduced in the duodenum, whereas in the jejunum a clear increase was detected, accompanied by a large standard deviation due to individual variability in one of the animals. In the ileum and colon, the levels remained intermediate and relatively close to each other. For both the M and cChAT, the highest standard deviation was observed in the duodenum, indicating substantial interindividual variability and suggesting the involvement of local regulatory mechanisms or physiological differences. Despite the absence of statistically significant differences, the results indicate a trend toward decreasing expression of the isoforms along the GIT in the distal direction, most notably in the colon. This trend may have biological significance, reflecting the different functional roles of the ENS in distinct segments of the gastrointestinal tract. In the proximal regions (duodenum and jejunum), the higher expression of ChAT is likely associated with more intensive cholinergic regulation of motor and secretory activity, which is critical for the initial stages of digestion. In contrast, the reduced expression in the distal parts of the GIT, particularly in the colon, may be interpreted as a reflection of a different pattern of neuronal regulation, in which alternative mediator systems (e.g., serotonergic or peptidergic signaling) play a greater role. These observations highlight the need for further studies to clarify the mechanisms underlying the observed interindividual variability and regional differences in the expression of ChAT splicing isoforms.

#### V. Conclusion

Acetylcholine is a principal neurotransmitter regulating diverse processes in both the somatic and autonomic nervous systems. The cholinergic system plays a central role in motor function, emotional behavior, and higher cognitive processes, including learning and memory. Alterations in cholinergic neurotransmission within the ENS are associated not only with functional gastrointestinal disorders but also with the pathophysiology of neurodegenerative diseases.

A reliable marker for visualizing cholinergic structures is the enzyme ChAT. Modern molecular approaches exploit splicing isoforms of ChAT mRNA, which are transcribed from the ChAT gene. The presence of multiple splicing isoforms increases the coding potential of the genome and the functional diversity of the proteins synthesized. In mice, seven isoforms – M, N1, N2, R1, R2, R3, and R4 – are transcribed from the 5'-noncoding region, while two additional isoforms, cChAT and pChAT, result from alternative splicing in the 3'-coding region. In the present study, we detected expression of the M, cChAT, and pChAT isoforms in the ENS along the entire length of the mouse GIT.

Investigating the splicing isoforms of enzymes involved in acetylcholine synthesis and elucidating the precise mechanisms by which the ENS contributes to disease pathogenesis will facilitate the development of cholinergic pharmacological and gene therapy strategies for conditions associated with cholinergic excess or deficiency.

Finally, although the mouse is not a perfect model for human biology, our approach – employing a minimal number of experimental animals combined with highly specific genetic resources – represents an effective and ethical strategy for obtaining meaningful insights into cholinergic function and gastrointestinal physiology.

#### VI. Deductions

In fulfillment of the objectives of this dissertation – namely, tracing the histological structure of the GIT wall and studying the expression of splicing isoforms of ChAT mRNA – the following main conclusions were drawn:

- 1. The Swiss roll method proved to be an efficient and optimal approach for histological analysis of large sections along the course of the mouse GIT. This technique allows to reveal histological features of the digestive tract wall through a series of cross-sections within a single preparation, facilitating both visualization and comparative analysis.
- 2. In the course of the genetic analysis, primer design for the R2 proved impossible due to its high homology to the other R isoforms and the lack of unique primer binding sites in the splicing isoform. Primer pairs were generated for the R1 and R4 isoforms, but due to the high similarity in nucleotide sequences with the R3 variant (for R1) and R3, N1 and M (for R4), amplification was also reported in control reactions of these primers with the templates corresponding to their homologous isoforms, which proved the non-specificity of the generated primers.
- 3. The designed *de novo* primer pairs to detect M, cChAT and pChAT successfully amplified specific PCR products of the expected length. The results of electrophoretic analysis confirmed the specificity of the amplification curves obtained by qPCR. There was complete agreement between the results obtained with synthetic arrays (gBlock1 and gBlock2) and those from reactions with isolated tissue cDNA. In the analysis of the R3 variant, although specific primers were used, only primer dimers were obtained, confirming the absence of this isoform in the ENS of adult C57Bl/6NCrl mice. Relative quantitative analysis of the expression of M, cChAT and pChAT in consecutive segments of mouse GIT showed no statistically significant differences in expression levels. This suggests a relatively even distribution of these isoforms along the ENS. The failure to identify N, and R-splicing isoforms suggests that they are absent or expressed at very low levels in the GIT tissues of adult mice, which contrasts with their increased expression during embryonic development.

#### VII. Contributions

## Contributions of an original nature

- 1. Conducted, for the first time, a systematic analysis of ChAT splicing isoform expression across all anatomical segments of the mouse GIT using molecular genetic methods.
- 2. Confirmed the expression of the common ChAT isoform (cChAT) in the ENS, traditionally associated with the CNS, expanding the understanding of its localization and potential functions outside the CNS.
- 3. Verified the expression of the peripheral ChAT isoform (pChAT) in the ENS, consistent with its established localization in structures outside the CNS, thereby supporting the ENS as a distinct cholinergic system.

### Contributions of applied nature

- 1. Designed optimal primer pairs for the detection of ChAT enzyme splicing isoforms, accounting for the high sequence similarity among isoforms.
- 2. Developed and optimized a quantitative qPCR protocol, including primer concentration, hybridization conditions, and DNA template amount, to achieve high sensitivity and specificity.
- 3. Established, for the first time, a validated qPCR protocol specifically targeting the detection of different ChAT splicing isoforms in the enteric nervous system of the mouse.
- 4. Created an Excel-based formula for automated fold change calculation that minimizes the risk of errors in manual calculations. This tool has an applied character as it facilitates the processing of experimental data and increases the accuracy of the analysis.
- 5. Performed relative quantitative analysis of ChAT splicing isoform expression across different segments of the mouse ENS.

## VIII. Future directions and perspectives

Tracking the expression profiles of different ChAT splicing isoforms in the ENS offers significant potential for advancing our understanding of cholinergic regulation in the peripheral nervous system. The results of the present study provide a foundation for future research that may inform the development of novel diagnostic markers and therapeutic strategies for conditions associated with impaired cholinergic function.

The following research directions are proposed:

- 1. Development and optimization of primer pairs for the specific amplification of R splicing isoforms of ChAT to enhance detection sensitivity and specificity.
- 2. Immunohistochemical and *in situ* hybridization analyses to localize ChAT isoforms at both the mRNA and protein levels within defined GIT compartments, providing detailed insight into their tissue- and cell-specific expression patterns.
- 3. Protein-level confirmation of splicing isoforms via Western blot, enabling differentiation based on molecular mass or isoform-specific antibodies.
- 4. Sequencing of PCR products to verify splicing structures and to identify potentially novel ChAT splice isoforms within the ENS.

Pursuing these directions will contribute to a more comprehensive understanding of the post-transcriptional regulation of ChAT and its role in both normal and pathological cholinergic signaling in the ENS.

## IX. Publications, participation in scientific forums and scientific project related to the dissertation

#### **Publications**

- **1. Marinova, D.,** Dobrev, M., Rashev, T., Gerasimov, I., Nankov, V., & Trifonov, S. (2022). Acetylcholine and its synthesizing enzyme choline acetyltranspherase in the enteric nervous system. *Journal of IMAB*, 28(4), 4671–4675. <a href="https://doi.org/10.5272/jimab.2022284.4671">https://doi.org/10.5272/jimab.2022284.4671</a> ISSN: 1312-773X.
- **2. Marinova, D.**, & Trifonov, S. (2024). Design of primers and optimization of PCR conditions for the detection of alternatively spliced isoforms of mouse ChAT mRNA. *Journal of Biomedical and Clinical Research*, *17*, 95-105. ISSN: 1313-6917.
- **3.** Glomus Coccygeum anatomical overview. Diagnostic and therapeutic significance, **Desislava M. Marinova**, Tihomir R. Rashev, Lyubomira D. Angelova, Nikola Gizdashki, Stefan V. Trifonov, 21st National Scientific Session for Students and Faculty "With a Vision for the Future", dedicated to the 75th anniversary of the establishment of the Medical College at the Medical University Pleven, 27-28.10.2023 Γ. 978-954-756-324-7 (CD/DVD).

#### Participation in scientific forums

- **1. Desislava M. Marinova**, S. Trifonov, T. Rashev, V. Nankov, I. Gerasimov, M. Dobrev. *In silico* PCR primer designing for specific identification of alternatively spliced isoform of ChAT mRNA in mice, Jubilee Scientific Conference, 31.10-02.11. 2019, Pleven.
- **2. Desislava M. Marinova**, K. Velikov, M. Dobrev, T. Rashev, S. Trifonov. The "Swiss roll a simple technique for histological visualization of the murine intestinal tract, XXV National Congress of the Bulgarian Anatomical Society, 28-30.05. 2021, Pleven.
- **3. Desislava M. Marinova**, T. Rashev, S. Trifonov, Testing of primers and optimization of PCR for the detection of alternatively spliced variants of mouse ChAT mRNA, XXVI National Congress of the Bulgarian Anatomical Society, 29.09-01.10. 2023, Sofia.
- **4. Desislava M. Marinova**, C. Popov, T. Raschev, S. Tfifonov, Diabetes-related alternations in the enteric nervous system, Jubilee Scientific Conference with International Participation, 1-3 November 2024, Pleven.

**Project № 25/2019 MU - Pleven** "Development and application of a specific quantitative PCR method for measuring the expression of alternative splicing variants of mRNA for the enzyme cholinacetyltransferase in mouse".

## Appendix 1

- I. Real time PCR–standard curve method
  - A. Preparation of standard curve for the absolute quantitation must know the exact copy number of the standard. 10-fold serial dilution with final concentrations 1.10<sup>6</sup>, 1.10<sup>5</sup>, 1.10<sup>4</sup>, 1.10<sup>3</sup>, 1.10<sup>2</sup>.

Sequence of the oligonucleotide used as template for the absolute standard curve:

## gBl-1\_ChAT, 699 bp

Stock solution is  $1 \text{ng/} \mu \text{l} = 1 \times 10^{-9} \text{ g/} \mu \text{l}$  of gBl-1.

1. Calculate the mass of a single molecule

$$m = \frac{\text{MW g/mol}}{6.023 \times 10^{23} molecules/mol}$$

 $6.023 \times 10^{23}$  – Avogadro's number (number of atoms of  $C^{12}$  in 1 mol of  $C^{12}$ ).

MW – molecular weight of the DNA fragment in g/mol

gBl-1 MW=431850.8 g/mol

$$m = \frac{431850.8 \text{ g/mol}}{6.023 \times 10^{23} \text{molecules/mol}} = 7.170028225.x \ 1010^{-19} \text{g/molecule}$$

2. Calculate the mass of the gBl-1 containing the copy-number of interest that is  $1x10^6$  to  $1x10^2$  copies.

#### mass of gBl - 1 needed = copy - number of interest x mass of single plasmid

Copy-number	x 7.170028225x10 <sup>-19</sup>	Mass of gBl-1 (g)
1 000 000	X 7.170020223X10	7.170028225x10 <sup>-13</sup>
100 000		7.170028225x10 <sup>-14</sup>
10 000		7.170028225x10 <sup>-15</sup>
1 000		7.170028225x10 <sup>-16</sup>
100		7.170028225x10 <sup>-17</sup>

3. Calculate the concentration of gBl-1 needed to achieve the copy-number of interest. Divide the mass needed by the volume to be pipetted into each reaction (2  $\mu$ l).

Conv. number	Mass of aP1 1 (a)		Final concentration of gBl-1
Copy-number	Mass of gBl-1 (g)		(g/µl)
1 000 000	7.170028225x10 <sup>-13</sup>		3.585014113x10 <sup>-13</sup>
100 000	7.170028225x10 <sup>-14</sup>	÷ 2 μ1	3.585014113x10 <sup>-14</sup>
10 000	7.170028225x10 <sup>-15</sup>		3.585014113x10 <sup>-15</sup>
1 000	7.170028225x10 <sup>-16</sup>		3.585014113x10 <sup>-16</sup>
100	7.170028225x10 <sup>-17</sup>		3.585014113x10 <sup>-17</sup>

## 4. Prepare the serial dilution of gBl-1.

 $C_1V_1=C_2V_2$ 

#	Source	Initial	Volume	Volume of	Final	Final conc. in (g/µl)	Resulting
ion	of gBl-1	conc.	of gB1	diluent (µl)	volume		copy-
Dilution	for	(g/μl)	(µl)		$(\mu l)$		number of
Di	dilution						gBl-1/2μl
S	stock	1.10-9	1 μ1	99 μl dH <sub>2</sub> O	100 µl	1x10 <sup>-11</sup>	NA
1	#S	1.10 <sup>-11</sup>	3.59 µl	96.41 µl	100 µl	3.585014113x10 <sup>-13</sup>	
1	πο	1.10	3.39 μ1	TE buffer	100 μ1	3.363014113X10	$1x10^{6}$
2	#1	3.59x10 <sup>-13</sup>	10 μ1	90 µl	100 µl	3.585014113x10 <sup>-14</sup>	
	$\pi$ 1	3.33810	10 μ1	TE buffer	100 μ1	3.363014113X10	$1x10^{5}$
3	#2	3.59x10 <sup>-14</sup>	10 μ1	90 µl	100 μ1	3.585014113x10 <sup>-15</sup>	
3	π2	J.J/X10	10 μ1	TE buffer	100 μ1	3.363014113X10	$1x10^{4}$
4	#3	3.59x10 <sup>-15</sup>	10 μ1	90 µl	100 µl	3.585014113x10 <sup>-16</sup>	
7	π3	3.33810	10 μ1	TE buffer	100 μ1	3.363014113X10	$1x10^{3}$
5	#4	3.59x10 <sup>-16</sup>	10 μ1	90 µl	100 µl	3.585014113x10 <sup>-17</sup>	
5	π <b>-1</b>	3.33810	10 μι	TE buffer	100 μ1	J.J0J01711JX10	$1x10^{2}$

#### gBl-2\_ChAT, 500 bp

Stock solution is  $1 \text{ng/} \mu \text{l} = 1 \text{x} 10^{-9} \text{ g/} \mu \text{l}$  of gBl-2.

5. Calculate the mass of a single molecule

$$m = \frac{\text{MW g/mol}}{6.023 \times 10^{23} molecules/mol}$$

gBl-2 MW=308844.1.8 g/mol

$$m = \frac{308844.1 \text{ g/mol}}{6.023 \times 10^{23} \text{molecules/mol}} = 5.12774531 \times 10^{-19} \text{ g/molecule}$$

6. Calculate the mass of the gBl-2 containing the copy-number of interest that is  $1x10^6$  to  $1x10^2$  copies.

## mass of gBl - 2 needed = copy - number of interest x mass of single plasmid

Copy-number	x 5.12774531x10 <sup>-19</sup>	Mass of gBl-2 (g)
1 000 000	X 3.12// +331X10	5.12774531x10 <sup>-13</sup>
100 000		5.12774531x10 <sup>-14</sup>
10 000		5.12774531x10 <sup>-15</sup>
1 000		5.12774531x10 <sup>-16</sup>
100		5.12774531x10 <sup>-17</sup>

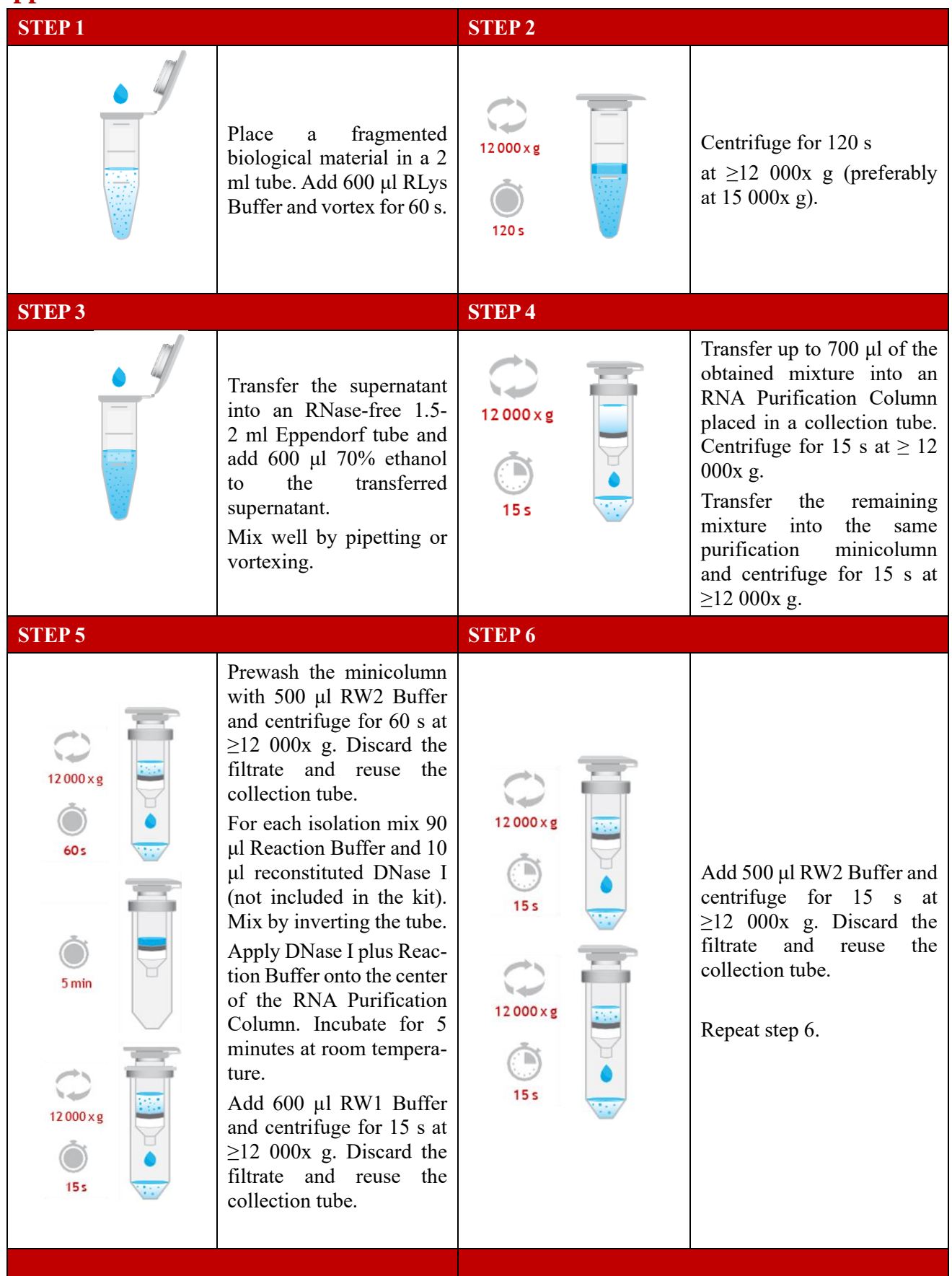
7. Calculate the concentration of gBl-2 needed to achieve the copy-number of interest. Divide the mass needed by the volume to be pipetted into each reaction (2  $\mu$ l).

Copy-number	Mass of gBl-2 (g)		Final concentration of gBl-2 (g/µl)
1 000 000	5.12774531x10 <sup>-13</sup>	. 21	2.563872655x10 <sup>-13</sup>
100 000	5.12774531x10 <sup>-14</sup>	÷ 2 μl	2.563872655x10 <sup>-14</sup>
10 000	5.12774531x10 <sup>-15</sup>		2.563872655x10 <sup>-15</sup>
1 000	5.12774531x10 <sup>-16</sup>		2.563872655x10 <sup>-16</sup>
100	5.12774531x10 <sup>-17</sup>		2.563872655x10 <sup>-17</sup>

# 8. Prepare the serial dilution of gBl-2. $C_1V_1{=}C_2V_2$

#	Source	Initial	Volume	Volume of	Final	Final conc. in (g/µl)	Resulting
lon	of gBl-2	conc.	of gBl-2	diluent (µl)	volume	,	copy-
Dilution	for	(g/µl)	(µl)		$(\mu l)$		number of
Di	dilution						gB1-2/2μ1
S	stock	1x10 <sup>-9</sup>	1 μ1	99 μl dH <sub>2</sub> O	100 μ1	1.10 <sup>-11</sup>	NA
1	#S	1x10 <sup>-11</sup>	2.56 µl	97.44 μl	100 µl	2.563872655x10 <sup>-13</sup>	
1	πυ	1710	2.30 μ1	TE buffer	100 μ1	2.303672033X10	$1x10^{6}$
2	#1	2.56x10 <sup>-13</sup>	10 μ1	90 µl	100 µl	2.563872655x10 <sup>-14</sup>	
	// 1	2.30x10	10 μ1	TE buffer	100 μ1	2.303072033X10	$1x10^{5}$
3	#2	2.56x10 <sup>-14</sup>	10 µl	90 µl	100 µl	2.563872655x10 <sup>-15</sup>	
3	πΔ	2.30x10	10 μ1	TE buffer	100 μ1	2.303072033X10	$1x10^{4}$
4	#3	2.56x10 <sup>-15</sup>	10 µl	90 µl	100 µl	2.563872655x10 <sup>-16</sup>	
	113	2.30x10	10 μ1	TE buffer	100 μ1	2.505072055X10	$1x10^{3}$
5	#4	2.56x10 <sup>-16</sup>	10 µl	90 µl	100 µl	2.563872655x10 <sup>-17</sup>	
	π <b>-T</b>	2.30x10	10 μι	TE buffer	100 μ1	2.303072033X10	$1x10^{2}$

## **Appendix 2**



STEP 7		STEP 8		
12 000 x g 90 s	Centrifuge for 90 s at ≥12 000x g (preferably at 15 000x g).  Discard the collection tube and the filtrate and carefully transfer the purification minicolumn to a sterile RNase-free 1.5 ml Eppendorf tube.	12 000 x g 60 s		Add 50-100 µl elution buffer REB. Centrifuge for 60 s at ≥ 12 000x g to elute purified RNA.  The isolated RNA is ready for use in downstream applications.